

**USE OF CONTOUR METHOD FOR ASSESSMENT OF RESIDUAL STRESS IN  
SUBMERGED ARC WELDING OF A36 STEEL**

A Thesis

by

LANG SHI

Submitted to the Office of Graduate and Professional Studies of  
Texas A&M University  
in partial fulfillment of the requirements for the degree of

MASTER OF SCIENCE

Chair of Committee,	Wayne Nguyen P. Hung
Co-Chair of Committee,	Bruce Tai
Committee Members,	Alan B. Palazzolo
	Angie H. Price
Head of Department,	Andreas A. Polycarpou

May 2018

Major Subject: Mechanical Engineering

Copyright 2018 Lang Shi

## **ABSTRACT**

This research presents a method to measure and calculate residual stress in A36 steel after submerged arc welding. Finite element is used to simulate the welding process and is compared with experimental data. After depositing beads on rectangular steel blocks, wire electrical discharge machining was used to section the blocks and welding bead in three orthogonal directions. The deformed surfaces due to releasing residual stress were measured using 3D optical technique. The surface topographies were used as boundary conditions in finite element analysis to calculate resulting residual stresses. The residual stress profiles from experiments and simulation are about 90% in agreement.

## **CONTRIBUTORS AND FUNDING SOURCES**

### *Part 1, faculty committee recognition*

This work was supervised by a thesis committee consisting of Professor Wayne Nguyen P. Hung from the Department of Mechanical engineering & Department of Engineering Technology & Industrial Distribution, Professor Bruce Tai from the Department of Mechanical engineering, Professor Alan B. Palazzolo from the Department of Mechanical engineering, and Professor Angie H. Price from the Department of Engineering Technology & Industrial Distribution.

### *Part 2, student/collaborator contributions*

Mr. Scott Butler from Department of Engineering Technology & Industrial Distribution assisted with the submerged arc welding experiments in Section 4 Experiments.

All other work conducted for the thesis was completed by the student independently. There was no outside source funding.

## NOMENCLATURE

$C$	Specific heat (J/kg/°C)
$I$	Current (A)
$K$	Kerf (mm)
$L$	Length (mm)
$Q$	Heat generation rate (J/s/m <sup>3</sup> )
$r$	Radial distance from center of the heat source (mm)
$R$	Region in which 95 % of the heat flux is deposited (mm)
$t$	Time (s)
$T'$	Temperature (° C)
$T$	Thickness (mm)
$U$	Voltage (V)
$v$	Welding speed (mm/s)
$W'$	Thermal conductivity (W/ (m° C))
$W$	Width (mm)
$x$	Coordinate X (mm)
$y$	Coordinate Y (mm)
$\eta$	Thermal efficiency
$\sigma_{x,y,z}$	Normal Stress in X, Y, Z directions (Pa)
$\rho$	Density (kg/m <sup>3</sup> )
$\beta$	Thermal expansion coefficient (mm/mm/° C)
$q(r)$	Surface flux at radius r (W/m <sup>2</sup> )

$q_{max}$  The largest heat input (J)

**Acronym**

APDL ANSYS Parametric Design Language

EDM Electrical Discharge Machining

FEA Finite Element Analysis

GUI Graphical User Interface

MRR Material Removal Rate

SAW Submerged Arc Welding

XRD X-Ray Diffraction

## TABLE OF CONTENTS

	Page
ABSTRACT .....	ii
CONTRIBUTORS AND FUNDING SOURCES.....	iii
NOMENCLATURE.....	iv
TABLE OF CONTENTS .....	vi
LIST OF FIGURES.....	viii
LIST OF TABLES .....	xii
1. INTRODUCTION.....	1
2. LITERATURE REVIEW.....	2
2.1 Residual stress .....	2
2.2 Submerged arc welding (SAW) .....	9
2.3 Contour method.....	10
3. FINITE ELEMENT SIMULATION OF SUBMERGED ARC WELDING .....	19
3.1 Thermal analysis .....	22
3.2 Stress analysis .....	33
3.3 Stress distribution.....	34
4. EXPERIMENTS .....	42
4.1 Overall experiment description .....	42
4.2 Submerged arc welding.....	42
4.3 Cutting process.....	47
4.4 Measuring surface .....	53
5. RESULTS AND DISCUSSION .....	57
5.1 Data processing .....	57
5.2 Stress calculation from experiments.....	62
5.3 Comparison of contour method and simulation .....	69
5.4 Compare with published data.....	73

6. CONCLUSIONS AND RECOMMENDATION.....	77
REFERENCES.....	78
APPENDIX A ANSYS PARAMETRIC DESIGN LANGUAGE (APDL) CODING FOR SUBMERGED ARC WELDING SIMULATION.....	82
APPENDIX B ANSYS APDL CODING AND GUI GUIDE FOR RESIDUAL STRESS SIMULATION FROM EXPERIMENTS.....	99
APPENDIX C MAPLE CODING FOR DATA PROCESSING .....	107
APPENDIX D STEPS FOR OBTAINING DATA FROM ALICONA .....	115
APPENDIX E EXPERIMENT FOR TESTING THE VALIDITY OF MAPLE CODING .....	122

## LIST OF FIGURES

	Page
Figure. 2.1. Weld thermal cycle of a) Location A, B and C. b) Temperature and Time relation of A, B and C .....	4
Figure. 2.2. Effect of temperature on variation in stress and strain during welding .....	6
Figure. 2.3. a) Welded plate, b) Stress variation across the weld centerline at different locations and c) Temperature at different positions .....	7
Figure. 2.4. Typical problems associated with residual stress a) Distortion and b) Solidification crack .....	8
Figure. 2.5. Submerged arc welding setup .....	10
Figure. 2.6. Residual stress measuring techniques.....	11
Figure. 2.7. Superposition principle for the contour method. ....	13
Figure. 2.8. Fixture arrangement for the EDM cut of weld plate.....	15
Figure. 2.9. (Left) Surface 1 contour after interpolation to a common grid. (Right) Surface 2 contour after interpolation to a common grid .....	16
Figure. 2.10 Averaged surface of surface 1 and surface 2 .....	17
Figure. 3.1. Welding model with length $L$ , width $W$ , and thickness $T$ . ....	21
Figure. 3.2. Simulation model meshing. ....	28
Figure. 3.3. Gaussian heat source model.....	29
Figure. 3.4. Thermal boundary condition.....	31
Figure. 3.5. Structural boundary condition.....	33
Figure. 3.6. Transverse stress ( $\sigma_x$ ) on half weldment .....	35
Figure. 3.7. $\sigma_x$ on YZ-plane at $X = 0$ .....	36
Figure. 3.8. Distribution of transverse residual stress ( $\sigma_x$ ) along centerline.....	36
Figure. 3.9. Transverse residual stress ( $\sigma_x$ ) on YZ-plane at $X = 0$ , along $Z = -T/2$ .....	37



Figure. 3.10. Longitudinal residual stress ( $\sigma_y$ ) on XZ-plane at $Y = W/2$ , along $Z = -T/2$ .	38
Figure. 3.11. Distribution of longitudinal residual stress ( $\sigma_y$ ) along centerline.....	39
Figure. 3.12. Residual stress in thickness direction ( $\sigma_z$ ) on XY-plane at $Y = L/2$ , along $Z = -T/2$ .....	40
Figure. 3.13. Distribution of residual stress in thickness direction ( $\sigma_z$ ) along centerline	41
Figure. 4.1. Calibration setup .....	43
Figure. 4.2. Welding speed calibration. ....	44
Figure. 4.3. Experimental setup. ....	45
Figure. 4.4. Welded workpiece. ....	46
Figure. 4.5. Fixtures for EDM sectioning. (a) EDM table, (b) Clamps, (c) Supporting beam, and (d) Welded workpieces .....	47
Figure. 4.6. Wire EDM setup for sectioning along Z direction. (a) Wire guide, (b) Clamps, (c) Supporting beam, and (d) Welded workpieces.....	49
Figure. 4.7. Section along X direction. (a) EDM table, (b) Clamps, (c) Supporting beam, and (d) Welded workpieces.....	50
Figure. 4.8. Section along Z direction. (a) EDM table, (b) Clamps, (c) Supporting beam, and (d) Welded workpieces.....	50
Figure. 4.9. (a) Main cut parameter for EDM. (b) Trim cut parameter for EDM.....	52
Figure. 4.10 Scanning along X direction (transverse direction).....	55
Figure. 4.11. Cut surface contour on XY plane obtained by Alicona. ....	55
Figure. 5.1. Surface contour of a specimen after sectioning at $Y = W/2$ plane (a) before noise filtering and (b) after filtering.....	61
Figure. 5.2. Residual stress calculation flowchart.....	62
Figure. 5.3. Experiment meshed model for (a) $\sigma_y$ (b) $\sigma_x$ (c) $\sigma_z$ .....	65
Figure. 5.4. Displacement boundary condition for (a) $\sigma_y$ (b) $\sigma_x$ (c) $\sigma_z$ .....	66
Figure. 5.5 (a) Residual stress $\sigma_y$ profiles on XZ-planes at $Y = W/2$ , along $Z = -3.17$ , $-6.35$ , and $-9.51$ mm. (b) Residual stress $\sigma_x$ profiles on YZ-planes at $X = 0$ , along $Z =$	

-3.17, -6.35, and -9.51 mm. (c) Residual stress $\sigma_z$ on XY-planes at $Z = -T/2$ , along $Y = 6.35, 12.70, \text{ and } 19.05 \text{ mm}$ .....	68
Figure. 5.6. Comparison of longitudinal residual stress ( $\sigma_y$ ) along centreline at $Z = -T/2, Y = W/2$ .....	69
Figure. 5.7. Comparison of transverse residual stress ( $\sigma_x$ ) along centreline at $Z = -T/2, X = 0$ .....	71
Figure. 5.8. Comparison of residual stress ( $\sigma_z$ ) along centerline at $Z = -T/2, Y = W/2$ ..	72
Figure. 5.9. Distribution of longitudinal residual stress .....	74
Figure. 5.10. Distribution of transverse residual stress .....	75
Figure. 5.11. Exact residual stress distributions in three directions .....	76
Figure. E1. Program calibration. ....	122
Figure. E2. Scanned contour before tilting .....	123
Figure. E3. Contour after tilting. ....	124

## LIST OF TABLES

	Page
Table 3.1. Experimental conditions.....	21
Table 3.2. Thermal and mechanical properties of A36 steel.....	24

## 1. INTRODUCTION

The residual stress that occurs during the welding process is due to non-uniform volumetric change upon cooling. Tensile residual stress should be minimized to minimize fracture and fatigue of the material in service. In this research, submerged arc welding was adopted because it is widely applied in industries for its high welding rates with controllable welding speed.

Many ways of measuring the residual stress have been implemented, and they are divided into three types: destructive including contour method and sectioning technique, semi-destructive including hole-drilling technique and ring-core method, and non-destructive including X-ray diffraction method and neutron diffraction method. Contour method was chosen because it is simple to execute and is applicable to a wide range of material. Also, the cost of contour method is cheaper than other methods, such as X-ray diffraction method.

The objective of this thesis is to develop a reliable procedure to measure welding residual stresses using contour method and verifying with FEA (Finite Element Analysis). The scope of the thesis is to use submerged arc welding and A36 steel for workpiece material. For the contour method, a new non-contact surface scanning technique was adopted to measure surface deflection due to the release of residual stresses.

## **2. LITERATURE REVIEW**

Residual stress in materials has always been an important focus because it can considerably influence material performance and quality such as distortion, fatigue life, corrosion resistance, and so on. Harmful residual stress leads to a large expenditure due to repairing structure or worse still, causing the malfunction of the structure or equipment. For instance, after welding, harmful residual stress might exist in the weld, and it will lead to a large reduction of fatigue life [1]. This literature review examines the ongoing research regarding the cause of residual stress, distribution of residual stress after welding and how to measure the residual stress.

### **2.1 Residual stress**

Residual stress can be defined as those stresses that are remained in the component, which have been processed using either thermal methods or mechanical methods without presence of the external load. Basing on the size of material the residual stresses exist in, residual stress is usually categorized into three types, namely, Type I, Type II, and Type III. They are described in details as follows [2-3]:

- Type I refers to the macro residual stress that develops in the body of component that is larger than the grain size of the material.
- Type II refers to the micro residual stress that varies on the scale of individual grain.
- Type III refers to the micro residual stress that exists within a grain. It usually results from dislocation and other crystalline defects. It should be noted that this

type of residual stress is generated at the atomic level. Type II and Type III are both micro residual stress. These three types of residual stress can all exist in one component at any time.

Thermally generated residual stress can be categorized into macroscopic residual stress and microscopic residual stress. On a macroscopic level, thermally generated residual stress is often caused by non-uniform cooling or heating, such as welding and heat treatment. For welding, the basic principle of how residual stress develops can be understood from the Fig 2.1 [4]. Fig. 2.1 shows a butt weld of two plates. A bead is generated at left and moving towards the right. Considering three points A, B and C on the plates, it is clear to us that since A is the closest to the boundary, C is the furthest and B is in between. A will reach the highest temperature first and heat will propagate to C, thus C will take the longest time to reach a lower temperature. Hence, for a unit in a given volume of metal, the metal subject to higher temperature will have greater expansion. Therefore, for a specific time, the expansion at locations A, B and C will be different. This differential volume change will take place due to the disparate weld thermal cycle at three positions. Subsequently, the contraction would also be different after each position reaches its highest peak temperature and starts to cool down. During the process when the molten metal begins to cool down to room temperature, its shrinkage will be restricted because the surrounding metal might still be solid thus creating residual stress.

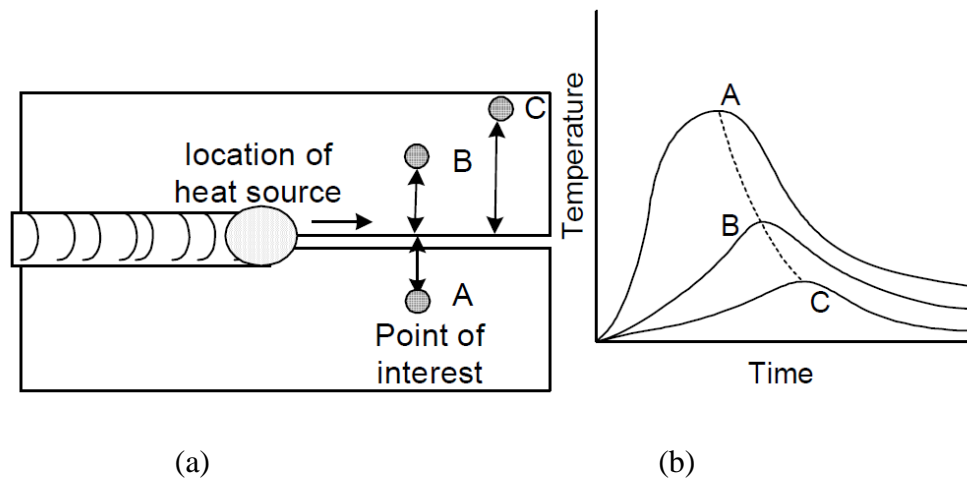


Figure. 2.1. Weld thermal cycle of a) Location A, B and C. b) Temperature and Time relation of A, B and C. Reprinted from [4].

As for microscopic stress, it is normally developed due to volumetric change occurring due to metallurgical transformations. (for example, austenite to martensitic transformation). Even though any types of transformation from the austenite to pearlite, bainite and the martensite may incur volume change, the transformation of austenite into pearlite and bainite are very limited in most cases, because the transformation requires higher temperature (usually higher than 550 °C). When the transformation from austenite to martensitic occur at a low temperature, higher magnitude of compressive residual stress develop due to this microscopic volume change during the cooling process [5].

The last process of producing residual stress is the chemical process. It is due to volume changes associated with phase transformation, precipitation, and chemical reactions. Chemical surface treatments and coatings can lead to residual stress in the surface layers of the component. For example, nitriding produces compressive stress in

the diffusion region due to the expansion of the lattice and the precipitation of nitrides [6].

If a point is randomly picked along the centerline of the weldment, the variation in stress and strain versus temperature can be illustrated using Fig 2.2 [7]. When the heat source comes close to the point of interest, temperature will rise. When the temperature rises, the metal being heated will experience thermal expansion. However, since the metal around it is still cold, it will limit the thermal expansion, resulting in the hot metal being compressed. This is the reason why the right side of Fig. 2.2 shows that, from point 1 to 2, the stress is negative (compressive stress). The left hand side of Fig. 2.2 illustrates how strain changes with temperature. It is worth noting that, with the increase of temperature, the yield strength decreases and the modulus of elasticity decreases. From point 2-3, when temperature gets higher, the metal starts to melt. The compressive stress will also begin to decrease gradually until it comes to point 3 where the compressive stress is zero. Then, after the heat source moves away, the metal starts to cool down and shrink. At the initial stage, since the temperature is still high and the yield strength is very low, the shrinkage is allowed. As a result, from point 4 to 5 on Fig. 2.2, the metal has no residual stress. The formation of residual stress is usually due to limitation of contraction or expansion. After the metal cools down and the yield strength gets higher, the shrinkage of metal is limited from surrounding cooler material. Subsequently, it will incur locked-in strain inside the metal. This process is described in Fig. 2.2 from point 5 to 6.



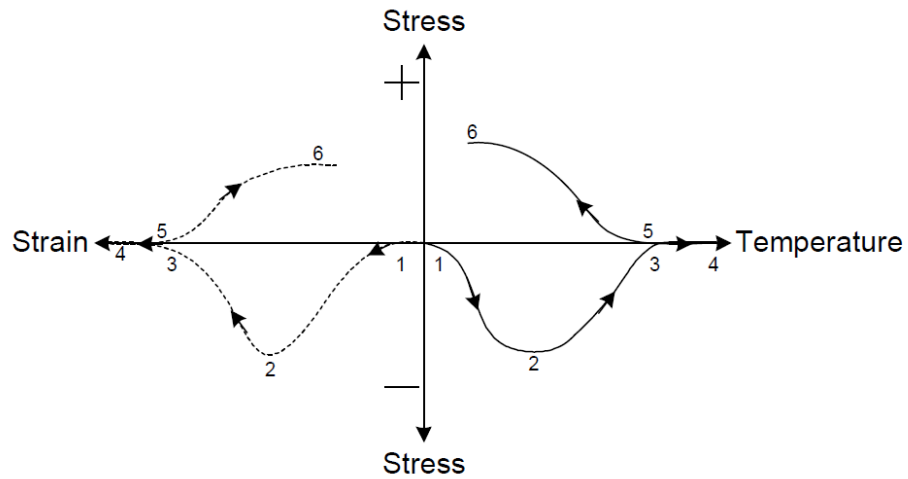


Figure. 2.2. Effect of temperature on variation in stress and strain during welding.

Reprinted from [7]

Since the overall stress should equal zero, residual stress along the weld is generally tensile in nature while the balancing compressive residual stress is developed adjacent to the weld, which is shown in the following Fig. 2.3. Consider a butt weld with a bead starting at the bottom and moving to the other end. We will find the temperature distribution and evolving stress at points E–A along the bead [7]. All the stress variation in b) is longitudinal residual stress distribution. When the metal plate is being welded, there are two types of shrinkage, longitudinal shrinkage and transverse shrinkage. These two directions are perpendicular to each other. The longitudinal direction is in the direction of the welding. The zone where the stress is tensile is called the tension zone. The adjacent area will have compressive stress (negative) that will balance out the tensile stress in the middle. The temperature graph at C also shows that the temperature

is relatively low. For position C, since the weld pool is barely beyond the threshold of position C, chances are the residual stress in the centerline is still compressive because it has not started to completely melt. This can also be indicated by looking at the temperature graph next to it because the temperature is still very high.

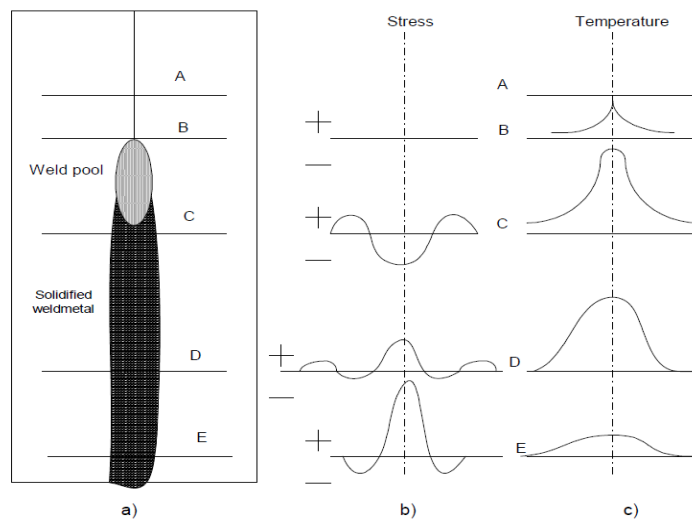


Figure. 2.3. a) Welded plate, b) Longitudinal stress variation across the weld centerline at different locations and c) Temperature at different positions. Reprinted from [7]

The existence of tensile residual stress in the weld could have adverse effect on weld joints, such as cracks (hot cracking, lamellar tearing, cold cracking), distortion (longitudinal, angular and transverse), and reduction in mechanical performance of the weld joint. The presence of residual tensile stress can encourage fracture due to external tensile loading. The cracking occurring at high temperatures is known as hot cracking.

Fig. 2.4 shows two typical problems associated with residual stress in two different pieces. Fig. 2.4 (a) shows longitudinal bowing in welded plates. It happens when the weld center is not coincident with the neutral axis of the section so that longitudinal shrinkage in the weld bends the section into curved shape. The top picture in Fig 2.4 (a) shows the pulling effect of weld below neutral axis whereas the picture below shows the pulling effect of weld above neutral axis (the dotted line stands for neutral axis). Fig 2.4 (b) shows solidification cracks which normally appear as straight lines along the centerline of the weld bead. There is two beads for comparison. The upper bead is intact after welding and the lower one shows the crack. The overriding cause of crack is that weld bead in the final stage of solidification has insufficient strength to withstand the contraction stress generated as the weld pool solidifies.

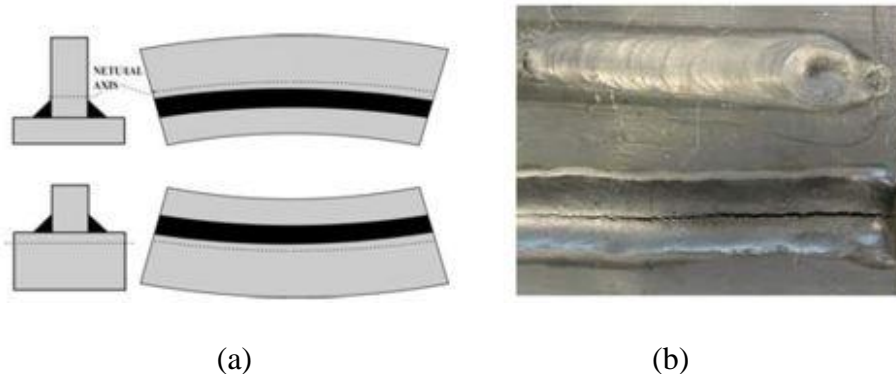


Figure. 2.4. Typical problems associated with residual stress a) Distortion and b)

Solidification crack. Reprinted from [7]

## **2.2 Submerged arc welding (SAW)**

Originally developed and patented by Jones, Kennedy and Rothermund, submerged arc welding process requires a continuously fed consumable solid or tubular (metal cored) electrode. It is a mechanized welding process that uses granular fusible flux to protect the molten zone and the arc zone. This is achieved by submerging the weld underneath the flux to prevent oxidation from surrounding air. In fact, since the welding process is underneath the blanket of flux, there will not be much spatter nor intense ultraviolet radiation that adversely affects an operator. The flux is made out of lime, silica, manganese oxide and other compounds, and it provides a current path between electrode and workpiece [8]. Since it is semi-automatic, SAW guarantees the consistency of the weld compared to other welding methods. It is semi-automatic in the sense that the welding process would go at a constant speed when the start and end of the process is specified. Submerged arc welding is used to weld low- and medium-carbon steels, low-alloy high-strength steels, quenched and tempered steels, and many stainless steels. As Fig. 2.5 shows, similar to GMAW welding, SAW involves formation of an arc between the wire electrode and the workpiece. Before the welding process starts, a thin layer of flux powder is placed on the workpiece surface. As the welding process proceeds, more flux will continue covering the path through the hopper. The remaining slag layers can be easily removed after welding.

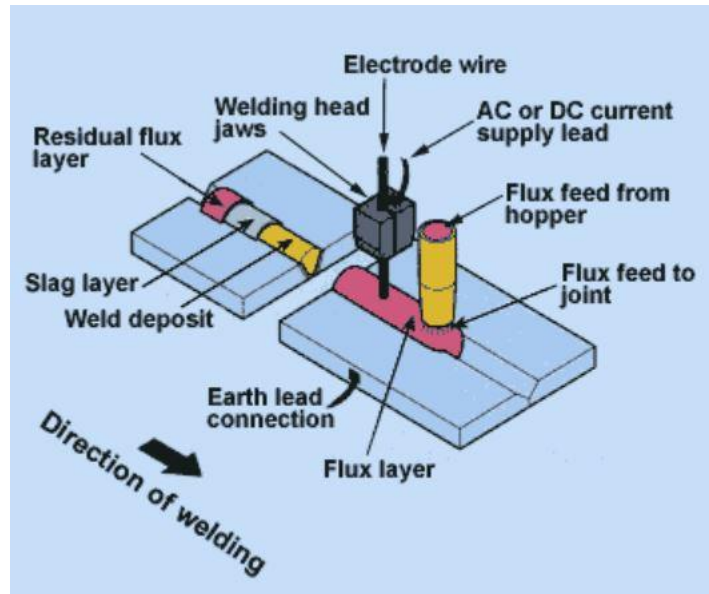


Figure. 2.5. Submerged arc welding setup. Reprinted from [9]

### 2.3 Contour method

Many ways of measuring residual stress (especially Type I residual stress) have been proposed over the years. They are categorized into three types: Destructive, semi-destructive, and non-destructive. The destructive and semi-destructive methods are also called mechanical methods because these methods rely on measuring the displacement of the material upon partially or completely releasing the residual stress. The detailed description of these methods can be represented by the following diagram [10]:

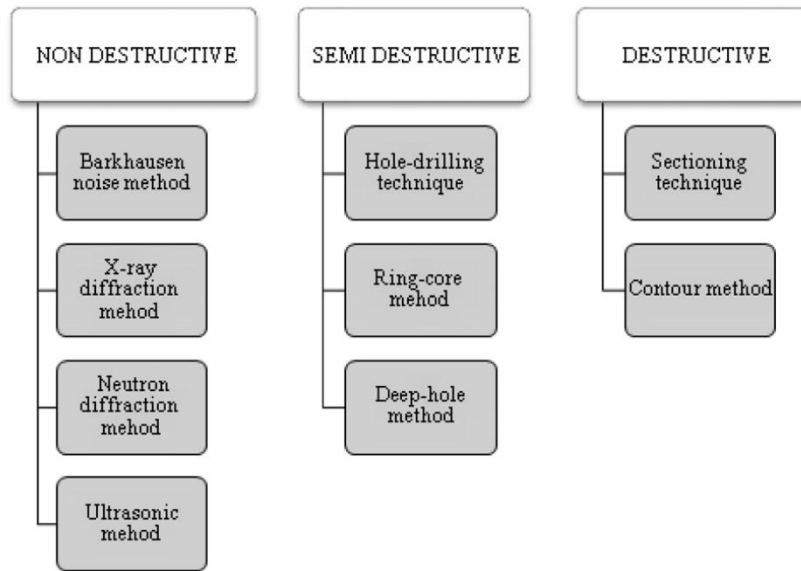


Figure. 2.6. Residual stress measuring techniques. Reprinted from [10]

Fig. 2.6 shows different techniques/methods within each category. The non-destructive methods have gained more attention recently, because they can measure residual stress without damaging the component itself. As a result, they are usually selected for the assessment of fatigue related inspections, such as bridges and aircrafts [11]. To determine the residual stress in those structural components, it is unwise to break and damage the component every time it needs periodical inspection. However, the non-destructive methods usually cost more than other methods.

The contour method is a destructive method of measuring residual stress based on solid mechanics. It determines residual stress in the specimen by cutting a piece into two and then measuring the deformation on the two surfaces resulting from the stress release. Bueckner's superposition principle [12] lays the foundation of the contour

method. According to this principle, if a cracked body subject to external loading or prescribed displacements at the boundary has forces applied to the crack surfaces to close the crack together, these forces must be equivalent to the stress distribution in an uncracked body of the same geometry, subject to the same external loading. The principle is clarified in Fig. 2.7 [13].

Fig. 2.7 demonstrates the ideal theoretical implementation of the contour method. Fig. 2.7 A shows the original residual stress built up inside along the longitudinal direction. Fig. 2.7 B shows that after the part is cut in two along the  $X = 0$  plane, the stress is released, resulting in stress in the  $X$  direction being 0. In Fig. 2.7 C, the deformed cut surface is forced back to its original shape, for which the displacement is exactly the opposite deformation of when the part is cut. Superimposing the stress state in B with the change in stress from C gives the original residual stresses in A:

$$\sigma^A(X, Y, Z) = \sigma^B(X, Y, Z) + \sigma^C(X, Y, Z) \quad (2.1)$$

$\sigma$  refers to the entire stress tensor at different steps. Since the stress at step B (free surface) is 0, we can uniquely determine residual stress in step A based on the stress value calculated in step C. The material is assumed to deform elastically after the part is cut in half and the cutting process does not introduce stress of significant magnitude to affect the measured stress.

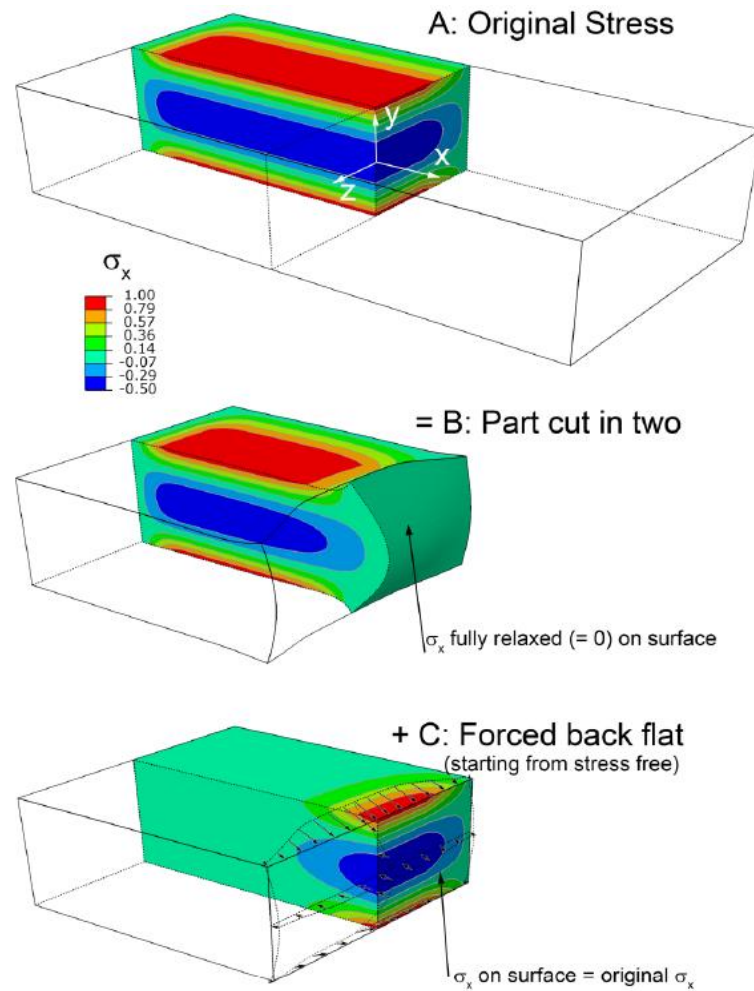


Figure. 2.7. Superposition principle for the contour method. Reprinted from [13]

The ideal machine for cutting the part is wire EDM. Wire EDM is a non-contact erosion process induced by the breakdown between the continuously feeding wire and work part. It can easily make a straight cut with a smooth surface and minimal cut kerf (usually only 110-120% of wire diameter). Also, it does not cause any plastic deformation like a conventional contact machining process would. After displacements



are obtained, a finite element model is built in ANSYS and displacements are imposed as a boundary condition on the model. One advantage of the contour method is that it provides an accurate two dimensional stress profile. Therefore, complex spatial variations of residual stress, which are typical of welds, can be well-characterized.

Normally, the sample is only clamped on one side, however, the application of the contour method is based on the relief of stresses that are normal to the cutting plane and any movement due to stress relief may change the shape of the plane. Thus, since the original plane of the cut should be constrained from moving as the stresses are relaxed during the cutting, clamping both sides of the cut of a rigid fixture is important. In general, the more clamps, the better, because clamping on only one side could induce “bulge error [14]” Since the cutting process made a cut of constant kerf width  $K$  in the reference frame, as the process proceeded, the stresses relaxed, and material at the tip of the cut deformed while the cut width remained  $K$ . The width of the cut had been reduced when measured relative to the original state of the body. One typical fixture arrangement for EDM cut is shown in Fig. 2.8. The weld plate is clamped by four clamps and the aluminum backing plate supports the weld plate. There is a pre-cut slot in the backing plate that allows for EDM wire to travel during cutting process.

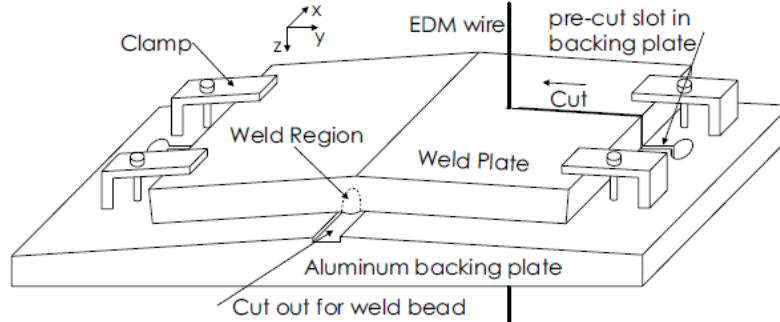


Figure. 2.8. Fixture arrangement for the EDM cut of weld plate. Reprinted from [15]

There are two types of cuts performed with wire EDM. They are “rough cuts” and “skim/trim cuts”. Rough cuts require higher voltage (along with other parameters) and have a higher material removal rate (MRR). Correspondingly, this cut has a pretty rough surface finish and proceeds much faster than “trim cuts”. “Trim cuts” are used to produce a high quality surface finish. “Trim cuts” have lower power and it has minimal recast (solidification of the molten area at the spark front) [13]. Generally, for an application, one or even two trim cuts are followed by a rough cut. However, this can cause some problem. The first being the large stress introduced by “rough cuts” because rough cut has a larger recast layer which induces stress and might reshape the surface. In addition, the second trim cut would remove the surface profile generated by the stress release of the first cut, resulting in inaccurate surface contour. For these reasons, one trim cut should be made through the sample. The speed of the trim cut could not be too fast because it might result in wire breakage.

After a specimen is cut, the measured data will contain errors from cutting; this is unavoidable. Averaging the contours can average away all the anti-symmetric cutting errors- those that cause a low spot on one side and a mating high spot on the other side. In an example demonstrated by Prime [15], after the cut by EDM, the data for surface 1 and surface 2 was aligned. This is shown in Fig. 2.9.

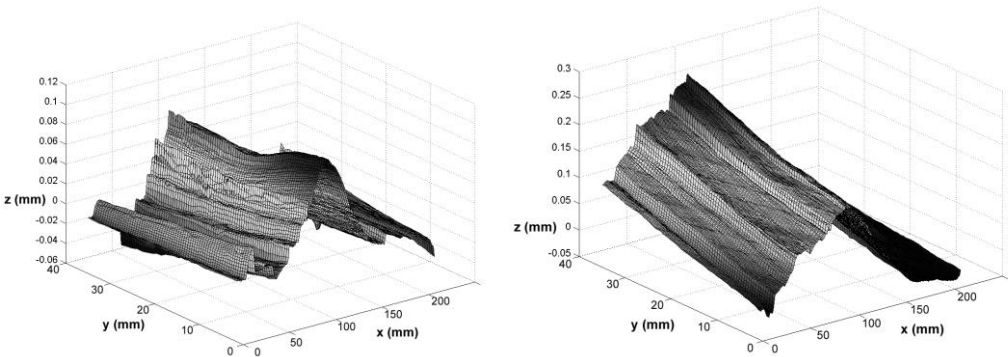


Figure. 2.9. (Left) Surface 1 contour after interpolation to a common grid. (Right) Surface 2 contour after interpolation to a common grid. Reprinted from [15]

The ridges at coincident locations from the two surfaces are due to wire EDM cutting. The two surfaces were then averaged together and the resulting surface is shown in Fig. 2.10, which has a very smooth surface relative to the contour in Fig. 2.9.

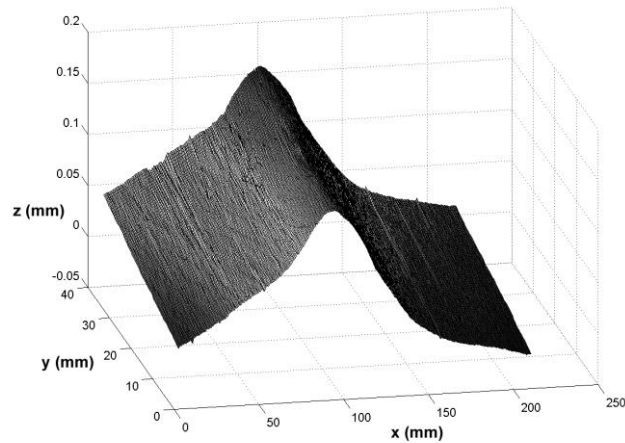


Figure. 2.10 Averaged surface of surface 1 and surface 2. Reprinted from [15]

There has been many investigators who have applied the different techniques to study the residual stress after welding. Olabi and Hashmi [16] used the hole drilling technique to measure the magnitude and the distribution of residual stress before and after application of post weld heat treatments of I-beam welded box-sections and high chromium steel AISI 410. They concluded that the soaking temperature has the major effect on diminishing the residual stress and, from 450°C to 650°C, the soaking temperature of 650 °C is most effective in reducing the residual stress from 360 MPa (tensile stress) to 10 MPa near the welding line.

Martinson et al. [17] applied neutron diffraction method in order to characterize residual stress after laser or resistance spot welding in automobile industry. They found that the weld region in laser spot welding was surrounded by a compressive region (180 MPa) which was higher than that in resistance spot welds (70 MPa). The laser welds

were made using a 3.3 kW Nd: YAG laser without shielding gas and filler wire were adjusted to obtain optimum joints. The resistance spot welds were made using a Schlatter 50 Hz AC stand alone spot welding machine. Spot welds were made with a nugget diameter of approximately 7.0 mm in the centre of a 40 mm overlap between the sheets and with 42 mm between spots.

Murugan and Narayanan [18] applied the contour method to evaluate residual stress of steel tee-joints. They adopted gas metal arc welding (GMAW) with an arc voltage of 30 V, welding current of 210 A and welding speed of 4.467 mm/sec to weld two pieces into a T joint. The two pieces have dimension of 210x100x5 mm and 210x50x5 mm. Tensile stresses were developed in the weld zone: the magnitude reached 400 MPa at the center, gradually decreased in the transverse direction away from weld center line, and became compressive residual stresses (up to 270 MPa) towards the edge of the plate.

### **3. FINITE ELEMENT SIMULATION OF SUBMERGED ARC WELDING**

In this section, a sequentially coupled, thermo-elastic plastic, three dimensional finite element computational procedure using ANSYS was developed to calculate temperature field and residual stress field. Firstly, a non-linear transient thermal analysis was carried out to determine the temperature field. Then the temperature histories obtained were used as part of the thermal boundary conditions to determine residual stress field.

For thermal analysis, ANSYS provides us with three types of methods [19], each of which is used in a different situation: Directly defined nodal temperature analysis is only used when the all the nodal temperatures are known, thus we can directly define nodal temperature through BF, BFE OR BFK commands. The other two methods are direct method and load transfer method. Since nodal temperature is normally not directly given, the second and third methods are often adopted. Direct method usually involves just one analysis using a coupled-field element type that contains all necessary degrees of freedom. Coupling is handled by calculating element matrices or element load vectors that contain all necessary terms. Load transfer method involves first obtaining temperature field and then using the results from the temperature field as the thermal load for structural analysis.

The difference between the direct method and the load transfer method lies in the fact that the direct method takes into account the bidirectional interaction between thermal and structural analysis. This means that the direct method not only takes into consideration how thermal analysis impacts stress analysis but also considers how, stress

analysis, in turn, influences thermal analysis. Usually, the stress field does not have much impact on the temperature field, especially when heat input is relatively small. Therefore, the load transfer method is adopted in the research.

The following are the main steps of welding simulation using ANSYS:

1. 3D finite element model: This includes the geometry of the model, the material properties and the meshing of the model.
2. Boundary conditions: This includes geometrical constraints, thermal constraints (pertaining to different environment) etc.
3. Moving heat source: This includes choosing suitable heat source model and implementing it during thermal analysis.
4. Time steps: This includes choosing the suitable time step for heat input and cooling phase.

The dimensions of the workpiece are 25.4 mm wide ( $W$ ), 76.2 mm long ( $L$ ), and 12.7 mm thick ( $T$ ) as shown in Fig 3.1. The material chosen is ASTM A36. One bead was run using autogenous welding. Since the stress profile would be symmetrical along the weld, the actual simulation model is half of the welding model shown in Fig.3.1.

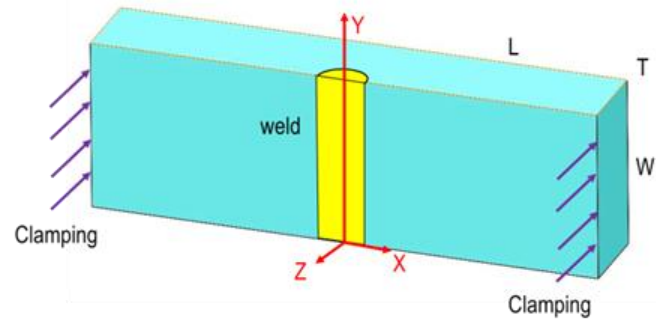


Figure. 3.1. Welding model with length  $L$ , width  $W$ , and thickness  $T$ .

The parameters for submerged arc welding are chosen as table 3.1 shows:

Parameter	Value
Welding speed	12.7 mm/s
Voltage	24 V
Current	400 A
Effective heat arc radius [21]	10.5 mm
Welding thermal efficiency [20]	0.85

Table 3.1. Experimental conditions.

In the submerged arc welding (SAW) process, it was assumed that the average arc efficiency to be  $0.84 \pm 0.04$  [20]. It was proposed that the effective arc radius ( $\sigma$ ) was 2.1 times that of the measured half bead width [21]. Since the average bead width was 10 mm, the effective arc radius would be 10.5 mm. If the travel speed is too low, there will be less



penetration; if too high, the weld will most likely have porosity and undercutting. 30 ipm is a very suitable speed (equals to 0.01267m/s). The normal amperage for submerged arc welding is within the range of 100-1300A. Since the workpiece is 12.7mm thick, 400A was chosen. The voltage is usually within the range of 20- 28V. A voltage setting of 24V was selected because the welding would be accomplished with one pass [22]. APDL coding for defining material properties is attached in Appendix A.

### **3.1 Thermal analysis**

#### **3.1.1 Determine geometrical model**

Normally, during the welding process, there is very complicated and intense physical and chemical reaction between the welding pool and the piece being welded. Those reactions involve fluid mechanics, heat transfer processes, and the interaction between the metal and heat source. This interaction between the metal and heat source includes the heat and pressure distribution over the work piece imposed by the arc, the surface deformation of the weld pool, and the evaporation of molten metal. When carrying out a simulation, it is very difficult to include all the reactions occurring during the welding process. Since this paper mainly focuses on the instantaneous change of temperature field and the resulting stress field, it is reasonable to ignore those factors that don't contribute to or have little influence on the temperature field and stress field. For example, for the fluid mechanics and heat transfer activities present in the weld pool, we only need to consider how the convection of liquid molten metal contributes to the

temperature field, instead of focusing on how the molten metal flows or how the gradient of surface tension varies during the welding process.

The following assumptions were made to simplify the simulation process:

1. The room temperature was assumed to be constant at 20 ° C.
2. The chemical reactions inside the weld pool, including stirring and convection, etc., were ignored.
3. The Gaussian distribution heat source model was utilized for submerged arc welding [23].

In ANSYS, if the geometrical model and loads are both symmetrical, then only half of the model needs to be simulated, which is true along the weld bead. Thus, only half of the model was analyzed in ANSYS.

### **3.1.2 Parameters of material properties**

The ASTM A36 plate was chosen as the base metal in this study. To carry out thermal analysis in ANSYS, it is necessary to know the following parameters of the base metal at different temperatures: thermal conductivity ( $\text{W/m}^\circ \text{C}$ ), density ( $\text{kg/m}^3$ ), specific heat ( $\text{J/kg}^\circ \text{C}$ ), initial temperature, melting points and the convection coefficient of the base metal. For stress analysis, additional parameters are needed, such as Young's modulus (GPa), yield stress (MPa), thermal expansion coefficient ( $^\circ \text{C}^{-1}$ ) and Poisson's ratio.

Welding simulation is a typical transient non-linear analysis. There are many materials that lack some necessary parameters at temperatures close to their melting

points. To solve this problem, we can input values of different properties at typical temperatures and use linear interpolation and extrapolation methods to obtain those unknown values at other temperatures. The thermal and mechanical material properties of ASTM A36 at different temperature are given in table 3.2:

Temperature (°C)	Specific heat (J/kg°C)	Conductivity (W/m°C)	Density (kg/m <sup>3</sup> )	Yield Stress (MPa)	Thermal Expansion Coefficient (10 <sup>-5</sup> /°C)	Young's Modulus (GPa)	Poisson's Ratio
0	480	60	7880	380	1.15	210	0.3
100	500	50	7880	340	1.2	200	0.3
200	520	45	7800	315	1.3	200	0.3
400	650	38	7760	230	1.42	170	0.3
600	750	30	7600	110	1.45	80	0.3
800	1000	25	7520	30	1.45	35	0.3
1000	1200	26	7390	25	1.45	20	0.3
1200	1400	28	7300	20	1.45	15	0.3
1400	1600	37	7250	18	1.45	10	0.3
1550	1700	37	7180	15	1.45	10	0.3

Table 3.2. Thermal and mechanical properties of A36 steel. Reprinted from [24]

The parameters listed in Table 3.2 were incorporated into the ANSYS simulation to get the temperature at every node using equation 1. The transient temperature during the welding process was determined by the three-dimensional nonlinear heat transfer equation [24]:

$$\rho C \frac{\partial T'}{\partial t} = \frac{\partial}{\partial X} \left( k \frac{\partial T'}{\partial X} \right) + \frac{\partial}{\partial Y} \left( k \frac{\partial T'}{\partial Y} \right) + \frac{\partial}{\partial Z} \left( k \frac{\partial T'}{\partial Z} \right) + Q \quad (3.1)$$

Where,

$\rho$ : density (kg/m<sup>3</sup>)

$C$ : specific heat (J/kg/°C)

$k$ : thermal conductivity (W/m/°C)

$Q$ : rate of internal heat generation (the Gaussian heat source) (J/s/m<sup>3</sup>)

$T'$ : temperature (°C)

$t$ : time (s)

$X, Y$  and  $Z$ : node coordinates (m)

### 3.1.3 Element type

Finite element method yields approximate values of the unknowns at a discrete number of points over the domain. To solve the problem, the method subdivides a large problem into smaller, simpler parts that are called finite elements. Every element is connected through nodes on which different types of loads are applied. Every node is a 3-D coordinate and it has different degrees of freedom. Finite element analysis is

intended to solve for the degree of freedom at every node. For thermal analysis, the degree of freedom of a node is temperature. For structural (stress) analysis, the degree of freedom is displacement. There are over 100 different types of element in ANSYS. The element chosen depends on different factors, such as whether the element is 2D or 3D, which kind of analysis is required, and how precise the final result is (at the cost of long computation time). In this paper, for thermal analysis, SOLID70 was chosen. SOLID70 is one of the most common element types for thermal analysis. SOLID70 has a three-dimensional thermal conduction capability. The element has eight nodes with a single degree of freedom, temperature, at each node. The element is applicable to a three-dimensional, steady-state or transient thermal analysis. The element also can compensate for mass transport heat flow from a constant velocity field. If the model containing the conducting solid element is also to be analyzed structurally, the element should be replaced by an equivalent structural element (such as SOLID185). Since the load transfer method was chosen, after thermal analysis, the analysis type transitioned into structural analysis while the element type switched to SOLID185. SOLID185 is used for three-dimensional modeling of solid structures because it has plasticity, stress stiffening, large deflection, and large strain capabilities. The element is defined by eight nodes having three degrees of freedom at each node: translations in the nodal  $X$ ,  $Y$ , and  $Z$  directions.

For this paper, PLANE55 was first introduced. PLANE55 can be used as a plane element or as an axisymmetric ring element with a two-dimensional thermal conduction capability. The element has four nodes with a single degree of freedom, temperature, at each node. We started the analysis using 2-D element type and then meshed the area,

after which it was extruded it into a three dimensional model (element type SOLID70) for thermal analysis [25].

### **3.1.4 Meshing**

There are two types of meshing in ANSYS, free meshing and mapped meshing. To generate a mapped mesh, the program can use all quadrilateral area elements, all triangle area elements, or all hexahedral (brick) volume elements. In free meshing operations, the model of any geometry, even if it is irregular, can be meshed. For area meshing, a free mesh can consist of only quadrilateral elements, only triangular elements, or a mixture of the two. For volume meshing, a free mesh is usually restricted to tetrahedral elements. Compared to mapped meshing, free meshing is generally easier to execute [26]. Since the geometry is rectangular, free meshing would be sufficient.

For finite element analysis, the finer the mesh, the longer the computational time will be and the more accurate the result will be. Conversely, the coarser the mesh is, the shorter the computational time will be and the less accurate the result will be. However, when the mesh is fine past a certain point, the result won't be more accurate if the mesh is made finer.

The welding process is an uneven heating process. The temperature gradient close to the bead changes very rapidly, but for the area far from the weld, the temperature gradient is smaller; thus when meshing, it is better to mesh finer close to the weld and use a coarser mesh far away from the weld. Therefore, one can both guarantee

an accurate result and save computational time. Generally, in order to obtain a fine mesh, the size of the mesh should be smaller than 2mm. For this research, the area is divided into four sections. The closest section to the weld has a mesh size of 0.8 mm. It is shown in Fig. 3.2:

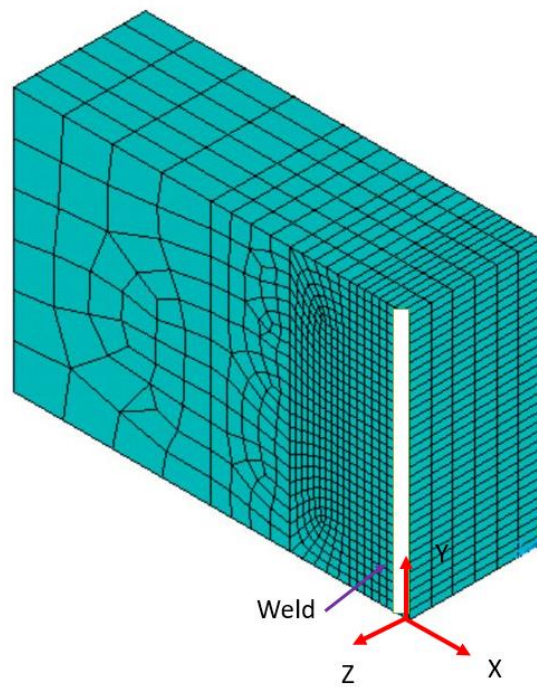


Figure. 3.2. Simulation model meshing.

The APDL commands for building 3-D model and meshing are attached in Appendix A.

### 3.1.5 Heat source

For most welding processes, the heat source is the most important boundary condition for thermal analysis. Because of localized heat input from the heat source, the temperature field induced by it is very unstable and non-uniform, resulting in residual stress built up inside the weld. Thus, it is important to choose a proper heat source model for the simulation. The Gaussian heat source is a model in which heat is generated over a surface and it is one of the most common heat sources adopted for welding simulation with thin plates and small heat input. In this paper, since the plate is only 12.7 mm thick, using the Gaussian model is sufficient. Fig. 3.3 depicts the Gaussian heat source model [23]:

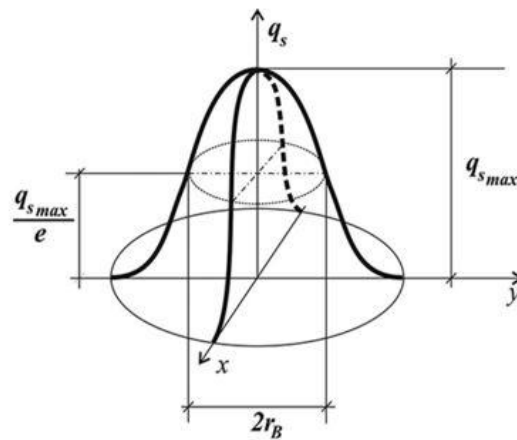


Figure. 3.3. Gaussian heat source model. Reprinted from [24]



It is clear in Fig. 3.2 that the heat input is greater in the center and heat intensity declines further away from the center of the heat source. The Gaussian heat source model can be described using following mathematical equation:

$$q(r) = q_{max} \exp\left(-3 \frac{r^2}{R^2}\right) \quad (3.2)$$

Where,

$q(r)$ : surface flux at radius  $r$  (W/m<sup>2</sup>)

$R$ : the region in which 95 % of the heat flux is deposited (mm)

$r$ : radial distance from center of the heat source (mm)

$q_{max}$ : the largest heat input (J)

$q_{max}$  is calculated as following [24]:

$$q_{max} = \frac{3}{\pi R^2} Q \quad (3.3)$$

$Q$  is the heat input and  $Q = U \times I \times \eta$ , with  $U$  being the voltage,  $I$  being the current and  $\eta$  being the arc thermal efficiency. All the parameters required to calculate surface flux at a certain point are given directly except for radius  $r$ , which can be calculated using the following equation:

$$r = \sqrt{x^2 + (y - v \times t)^2} \quad (3.4)$$

As Fig. 3.3 shows, the weld was travelling in the positive  $Y$  direction. The coordinate for the center of the heat source was be  $(0, v \times t)$ . Since the heat source

was traveling at speed  $v$  after time  $t$ . The coordinate for any point on the top surface was  $(X, Y)$ . Thus, the distance between the two points was given by equation (5). The commands for defining the parameters for welding and Gaussian function are attached in Appendix A.

### 3.1.6 Thermal boundary conditions

The most important boundary condition for thermal analysis is the Gaussian heat input. In addition, there is also the convection boundary condition between the workpiece and air.

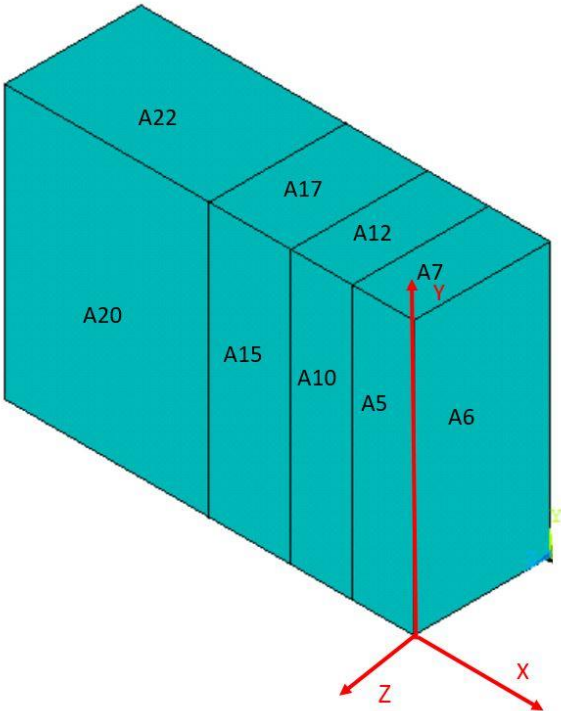


Figure. 3.4. Thermal boundary condition.

Fig. 3.4 shows the simulation model with areas number. A20, A15, A10, A5 are different is because the meshing is different. Finer mesh is close to the weld because temperature changes more rapidly. A6 is where the geometry was split in half, this means A6 is not exposed to air because only half the specimen was modeled; because of this, A6 does not have any initial thermal boundary condition. The thermal boundary conditions for areas A10 and A5 were mostly heat input from the heat source. For other areas, convection between the metal and air were imposed. The commands for imposing the thermal boundary condition are attached in Appendix A.

### **3.1.7 Time step**

During transient analysis, the load usually changes with time. The welding process was divided into 4 stages: welding and three-interval cooling. The first cooling interval with short time step while the second and third cooling interval with longer time step to save computing time.

- Welding at 12.7 mm/s across the specimen width of 25.4 mm. The welding time (2 s) was divided into 50 intervals of 0.04s per step.
- After weld cooling for 10s. This initial cooling time was divided into 80 intervals of 0.125s.
- The second phase cooling for 40s. This cooling time was divided into 60 sub-steps of 0.667s.

- Following cooling for 190s. This cooling time was divided into 100 intervals of 1.9s [27].

The commands for setting time step is included in Appendix A.

### 3.2 Stress analysis

After thermal analysis was completed, the next step was stress analysis. With the load transfer method, the temperature histories were imposed as thermal boundary condition for stress analysis. Before starting structural analysis, it was necessary to switch the element type from SOLID70 to SOLID185.

Fig. 3.5 shows the structural boundary conditions when the workpiece was clamped down:

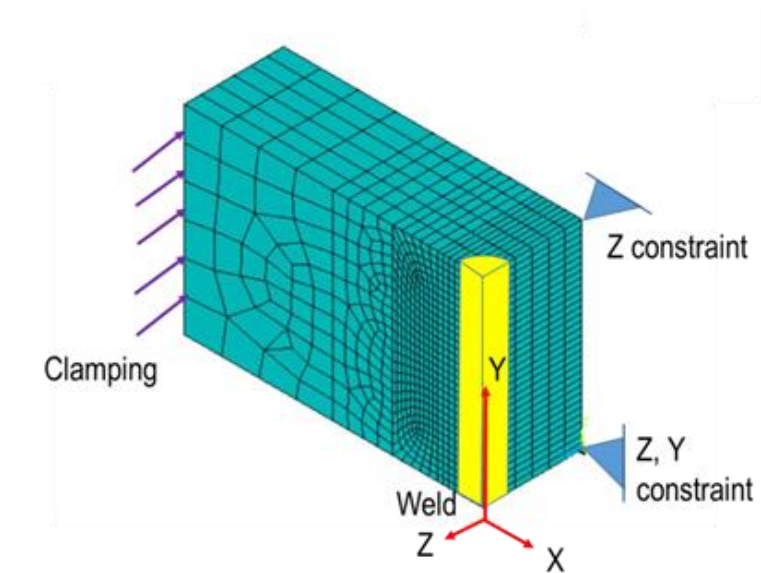


Figure. 3.5. Structural boundary condition.

Since half of the workpiece was modeled in ANSYS, the cut plane (symmetry plane) was fixed in the direction perpendicular to the weld line. Rigid body constraints were applied at two nodes on the cut plane to prevent rigid body translation. Since the piece was clamped down, the free edge of the plate was fixed in the direction perpendicular to the plate surface [28]. Stress analysis started after displacement boundary conditions were applied. The APDL coding is included in Appendix A.

### **3.3 Stress distribution**

#### **3.3.1 Transverse stress ( $\sigma_x$ )**

After stress analysis was completed, stress distributions along different directions inside the weld were plotted. The two-dimensional mapping of transverse residual stress is shown in Fig. 3.6. It shows that the transverse residual stress is tensile around the middle of the weld and is compressive towards the two ends of the weld.

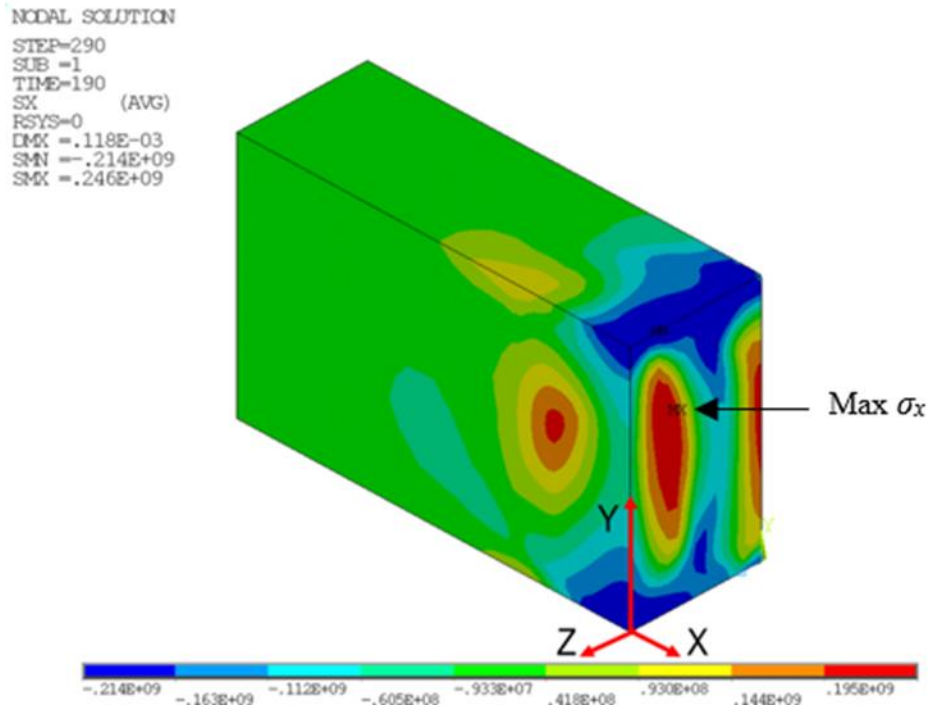


Figure. 3.6. Transverse stress ( $\sigma_x$ ) on half weldment

Transverse stress ( $\sigma_x$ ) variation along the centerline (YZ plane at  $Z = -T/2, X = 0$ ) is shown in Fig. 3.6. It shows the maximum stress of 246 MPa on the surface. The GUI instructions for obtaining such a graph is attached in Appendix B [29]. Fig. 3.7 shows the transverse stress at YZ cut plane at  $X = 0$ . Fig 3.8 shows the stress variation at  $Z = -T/2$  on YZ plane. Also, Fig. 3.9 superimposes  $\sigma_x$  along centerline onto the model.

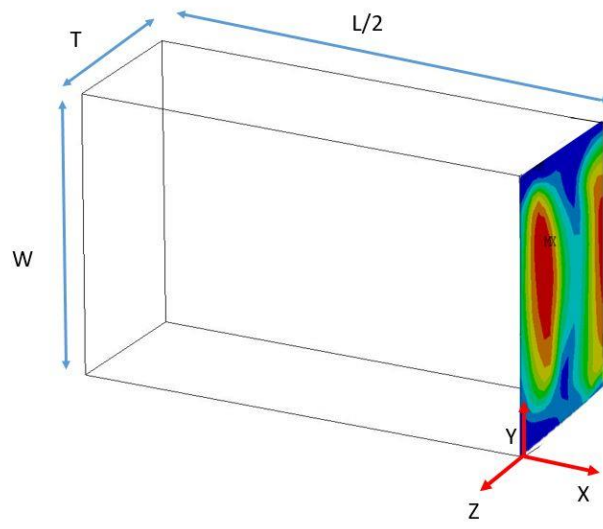


Figure. 3.7.  $\sigma_x$  on  $YZ$ -plane at  $X = 0$

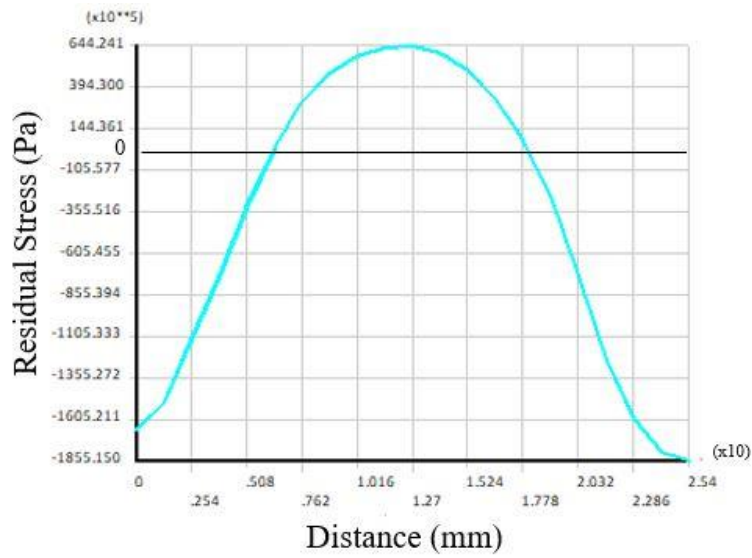


Figure. 3.8. Distribution of transverse residual stress ( $\sigma_x$ ) along centerline at  $X = 0$ , along  $Z = -T/2$

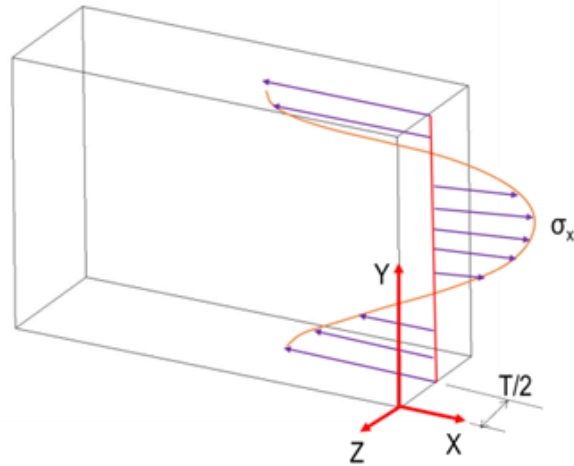


Figure. 3.9. Transverse residual stress ( $\sigma_x$ ) on YZ-plane at  $X = 0$ , along  $Z = -T/2$

### 3.3.2 Longitudinal stress ( $\sigma_y$ )

Longitudinal stress ( $\sigma_y$ ) inside the weld is defined as stress along the weld bead direction. In this model, in order to see the 2-D longitudinal stress profile, it was necessary to move the work plane to the middle and section the model in order to see the inside. The GUI instructions for moving the work plane and plotting the sectioned graph are attached in Appendix B. Fig 3.10 shows the 2-D mapping of  $\sigma_y$  on XZ plane at  $Y = W/2$  with the stress variation along centerline at  $Z = -T/2$ . Fig 3.11 displays the stress variation along the Y direction at XZ-plane at  $Y = W/2$ , along  $Z = -T/2$ . Positive residual stress are both tensile in Fig. 3.10 and Fig. 3.11.



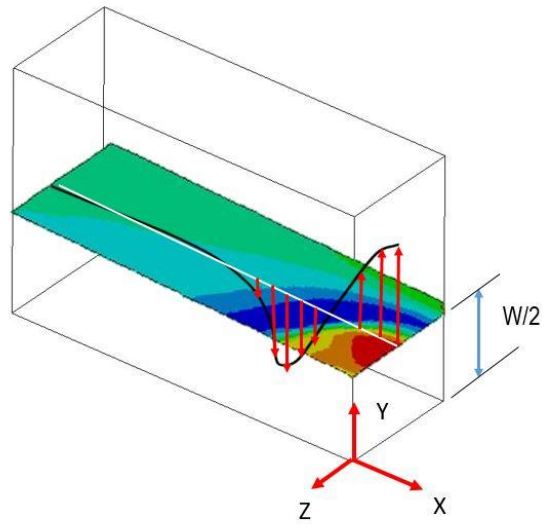


Figure. 3.10. Longitudinal residual stress ( $\sigma_y$ ) on XZ-plane at  $Y = W/2$ , along  $Z = -T/2$ .

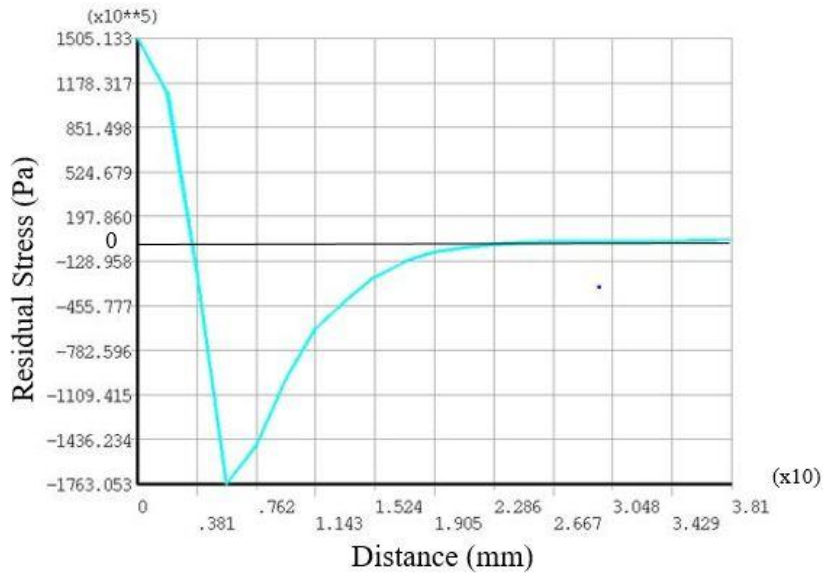


Figure. 3.11. Distribution of longitudinal residual stress ( $\sigma_y$ ) along centerline at  $Y = W/2$ , along  $Z = -T/2$ .

### 3.3.3 Stress along thickness direction ( $\sigma_z$ )

Fig 3.12 shows the 2-D mapping of residual stress along thickness direction  $\sigma_z$  on  $XY$  plane at  $Y = L/2$  with the stress variation along centerline at  $Z = -T/2$ . Fig 3.13 displays the stress variation along the  $Z$  direction at  $XY$ -plane at  $Y = W/2$ , along  $Z = -T/2$ . Tensile stress is positive in Fig. 3.12 and Fig. 3.13.

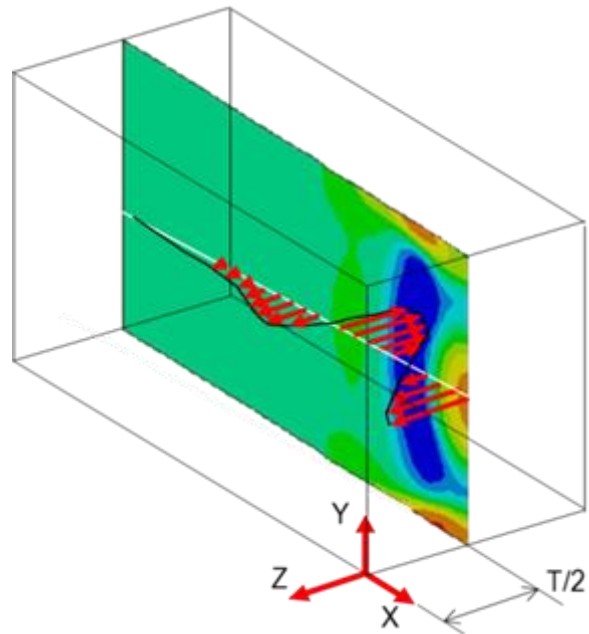


Figure. 3.12. Residual stress in thickness direction ( $\sigma_z$ ) on XY-plane at  $Y = L/2$ , along

$$Z = -T/2$$

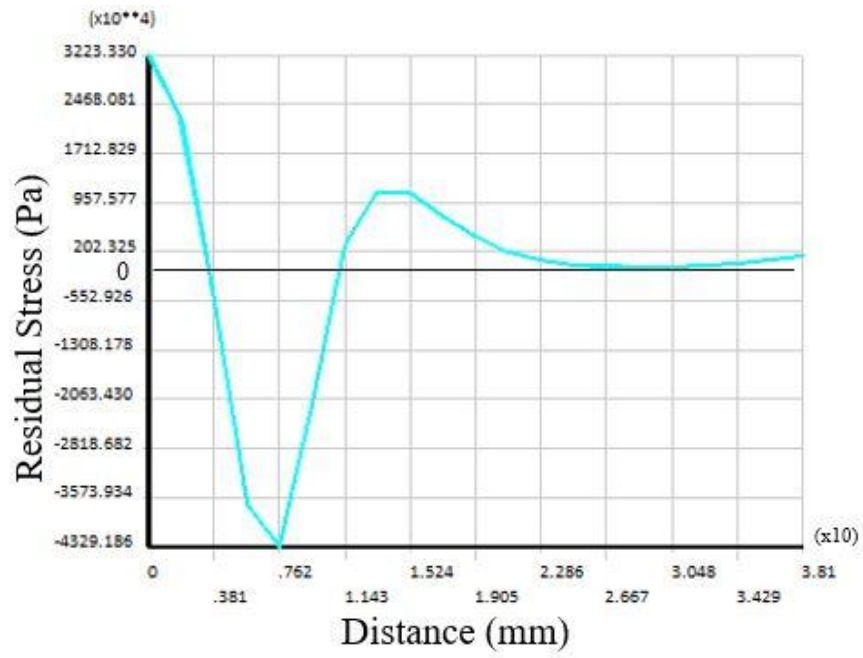


Figure. 3.13. Distribution of residual stress in thickness direction ( $\sigma_z$ ) along centerline at

$$Y = L/2, \text{ along } Z = -T/2.$$

## 4. EXPERIMENTS

### 4.1 Overall experiment description

The steps involved in the experimental procedure of the contour methods were as follows:

1. Welded the pieces using submerged arc welding.
2. Used wire EDM to cut in specified direction ( $X, Y, Z$ ) normal to the stress component ( $\sigma_x$  along  $YZ$  plane at  $X = 0$ ;  $\sigma_y$  along  $XZ$  plane at  $Y = W/2$ ;  $\sigma_z$  along  $XY$  plane at  $Z = -T/2$ ).
3. Measured the stress relieved surface contours using optical Alicona on the pair of cut surfaces and processed the data.
4. Built a finite element model in ANSYS that represent the cut sample.
5. Put in boundary conditions in the model and applied the negative of the displacement as a boundary condition normal to the model surface.
6. Applied the negative of the measured contour as a boundary condition normal to the model surface. According to Bueckner's superposition principle, this is the stress that was originally in sample prior to cutting.

### 4.2 Submerged arc welding

A submerged arc welding system utilizing an ESAB controller and an ESAB LAF 1000 DC power supply was used for the weld. A Weldwire manipulator was used for the travel of the weld head. The electrode was  $\phi 3.97$  mm ( $\phi 5/32$  inch) Lincoln L61, and the flux was Lincoln 860. A surface bead was made on A36 steel (98% Fe, 0.25-

0.29% C, 1.03 Mn, 0.04 P, 0.05 S, 0.280 Si, and 0.20 Cu) [30]. Prior to welding the specimens, calibration of welding speed was performed. To calibrate the welding speed, some scrap pieces were used to calibrate the robot welding speed to the 12.7 mm/s (Refer to Table 1 in Chapter 3). As Fig.4.1 shows, the table F should be ground first to ensure a better conductivity. The substrate B was clamped by E to the table F to close the circuit (the clamp was connected to the negative of power supply). Before the welding process started, the welding head A was moved to the top of the dummy piece C and a stopwatch was used to time the start and end of a known range, thus the welding speed was measured to be 12.7 mm/s.

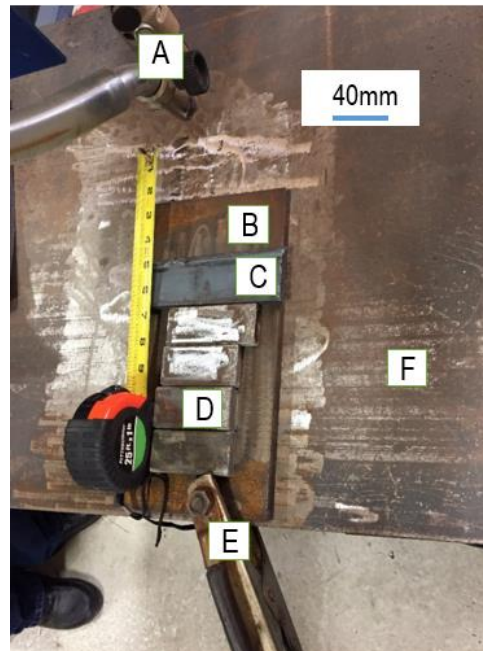


Figure. 4.1. Calibration setup. (A) Welding head (B) Substrate (C) Dummy piece  
(D) Specimen (E) Clamp (F) Table



Figure. 4.2. Welding speed calibration.

Fig. 4.2 shows the weld beads after two calibration passes (after the flux was removed). The left pass showed inconsistency at the beginning because the table and workpiece weren't ground so the rust on them resulted in bad conductivity. The same gap was left in between pieces; the width of the gap was around 0.5 mm. The second pass on the right shows great consistency and the speed was calibrated to be 12.7 mm/s.

After the welding speed was calibrated, the specimens were then welded. The base metal plate was an ASTM A108 steel, 12.7 mm thick, 152.4 mm wide and 304.8 mm long. The specimen was A36 steel. A specimen was milled from a cold rolled plate

to rectangular samples of 25.4 mm wide (W), 76.2 mm long (L), and 12.7 mm thick (T).

The specimens were rigidly clamped on the base plate before welding (Fig. 4.3).

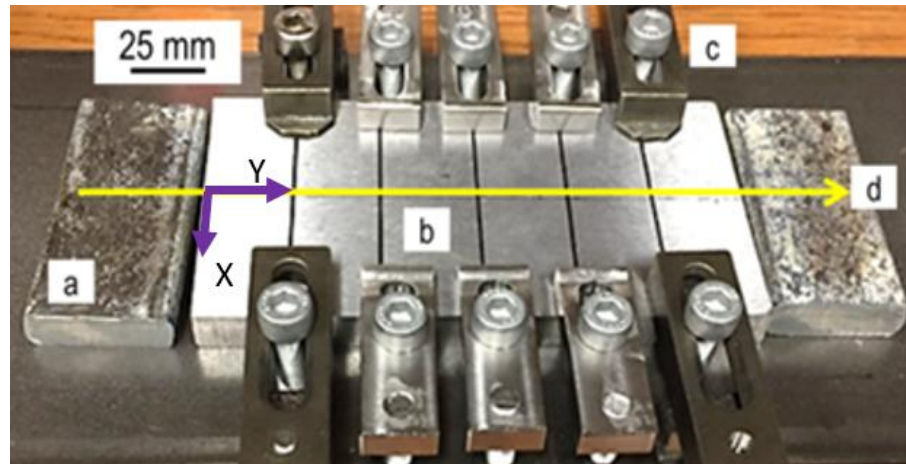


Figure. 4.3. Experimental setup. (a) Dummy piece, (b) Weld specimens, (c) Clamp, and (d) Weld direction.

A total of six specimens were used for each weld pass. Dummy specimens (75 x 40 x 13 mm) were placed at the beginning and end of specimen array to provide a path for welding head to accelerate to the desired speed and stabilize the welding arc. The origin was in the middle and at the weld entrance. All samples were rigidly clamped at both ends in the  $-Z$  direction. Shims of 0.5 mm thick were sandwiched between specimens for ease of specimen separation after laying a continuous bead. After welding, clamps were removed after 12 hours to ensure specimens didn't bow on the two ends.



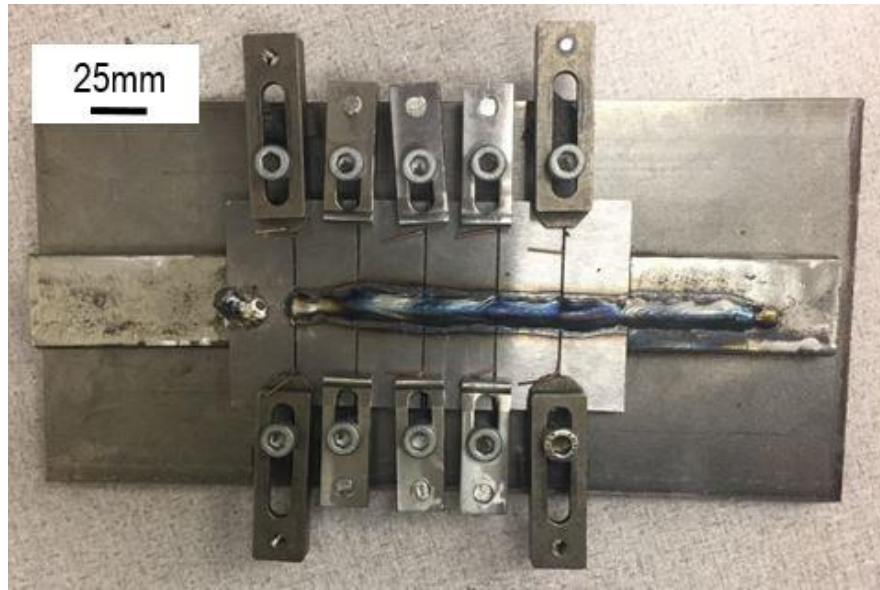


Figure. 4.4. Welded workpiece.

Figure 4.4 demonstrates the completed weldment with the flux removed. It can be clearly seen that the first piece on the far left side was not welded, and the second piece was not stable. This occurred because more distance than expected was required for the arc to stabilize. One reason could be that the left dummy piece had some rust on it, which caused the piece to connect badly to the table. The third to sixth pieces had a very consistent weld. This was sufficient for the analysis of the stress along the  $X$ ,  $Y$  and  $Z$  direction". (One extra piece will be used to the perform repeatability test for one direction).

### 4.3 Cutting process

After the welding process was completed, it was necessary to first section the individual pieces off and then section the individual pieces along X, Y, Z directions. The fourth piece was sectioned along X direction to confirm repeatability.

#### 4.3.1 Cutting procedure

The first step of the cutting process was to design the fixture. As Fig 4.5 shows, a supporting aluminum beam “c” was bolted to the EDM table “a”. Two clamps “b” were used on both sides of the workpiece to make sure it would not move during the sectioning process.

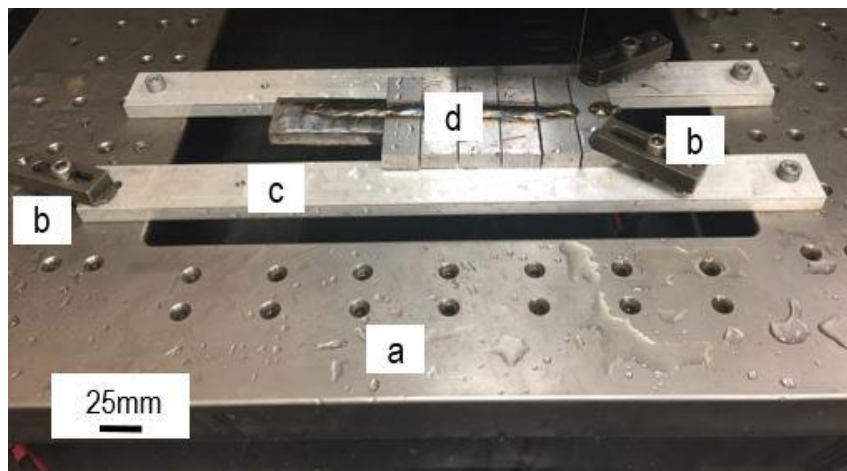


Figure. 4.5. Fixtures for EDM sectioning. (a) EDM table, (b) Clamps, (c) Supporting beam, (d) Welded workpieces

Two types of cuts associated with EDM, namely “rough cuts” and “skim/trim cuts”, were both performed. Rough cuts require higher voltage (along with other parameters) and have a higher material removal rate (MRR). Correspondingly, “Trim cuts” were used to produce a high quality surface finish. First, “rough cuts” were performed six times to section individual pieces. Then “trim cuts” were used four times to section individual samples along three orthogonal directions plus one for repeatability test. The parameters for achieving different cuts are explained in section 4.3.2.

The first cut was to separate the individual pieces. Cutting the weld was difficult because the material being cut was very inconsistent throughout the cut. Thus, higher voltage was supplied to the wire to cut it since it was easier to cut and it took less time. Fig 4.6 shows one setup for sectioning individual specimen off. Two pieces were sectioned vertically since it had shorter travel range thus saving time. Lifting components “b” were used to help clamp “c” to stabilize the workpieces during sectioning process. Lifting components “b” landed on the supporting beam “a” which was bolted to the sink table.

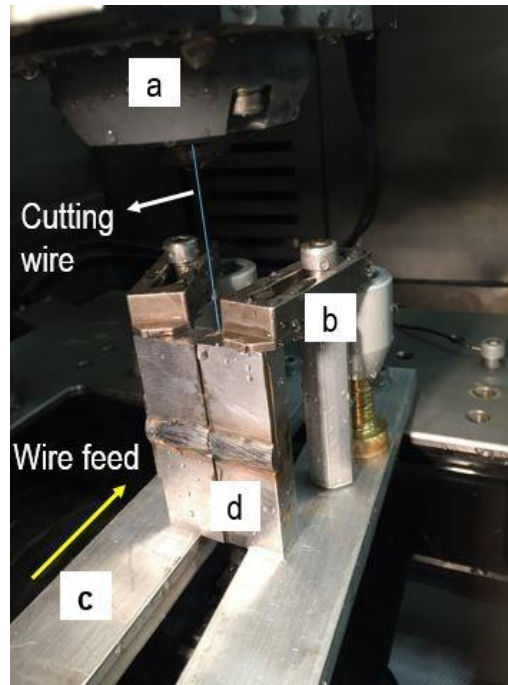


Figure. 4.6. Wire EDM setup for sectioning along Z direction. (a) Wire guide, (b) Clamps, (c) Supporting beam, and (d) Welded workpieces

After sectioning all the individual piece, three pieces were sectioned along three orthogonal directions. The following Fig 4.7 shows the section along the weld in X direction.

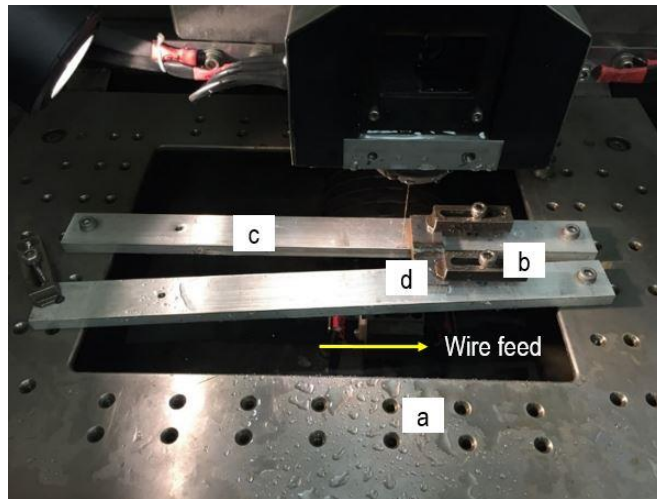


Figure. 4.7. Section along X direction. (a) EDM table, (b) Clamps, (c) Supporting beam, and (d) Welded workpieces

Fig. 4.8 shows the setup for sectioning along the Z direction (thickness direction):

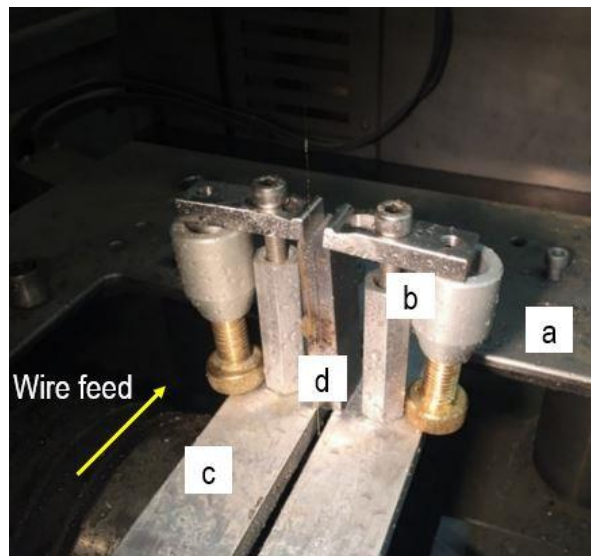


Figure. 4.8. Section along Z direction. (a) EDM table, (b) Clamps, (c) Supporting beam, and (d) Welded workpieces

After sectioning, the WD-40 lubricant was applied to cut surfaces to prevent rust formation. They were blown dried with compressed air before measuring cut surfaces.

#### **4.3.2 Parameter settings**

Two sets of parameters were used in the cutting process. The first set was used in the main cut for sectioning the individual pieces off, and the second set of parameter was used in the trim cut for cutting each individual piece along *X*, *Y*, *Z* directions. They are shown in Fig.4.9:

Page1

MODULE	0	WTy	Main
I	17	SPL	5
UHP	0	Ppos	0
ISH	-2	Pneg	1
P	50	Tmis	Default
Ton	32	Teros	Default
SSoll	30	VS	0.01
Reg	0	SMode	0
Str	55	<input checked="" type="checkbox"/> ACO	

(a)

Page1

MODULE	0	WTy	Trim
I	11	SPL	18
UHP	0	Ppos	1
ISH	0	Pneg	1
P	84	Tmis	3
Ton	32	Teros	10
SSoll	40	VS	13.00
Reg	F14	SMode	10
Str	0	<input type="checkbox"/> ACO	

(b)

Figure. 4.9. (a) Main cut parameter for EDM. (b) Trim cut parameter for EDM

Here are some explanation as to the meaning of different parameter settings:

- I: discharge current. This parameter is a big distinguisher between trim cuts and main cuts. When Module is set to be 00,  $I_{max} = 20$  A. When the discharge current goes up, it will increase cutting speed and roughness of the workpiece. Increase in current can also lead to a higher risk of wire break and geometric errors. This is the reason why trim cuts have a much lower discharge currents. (11 A vs 17 A)
- SSoll: SSoll is the reference parameter determining the optimum feed rate during erosion. Decreasing SSoll will increase the cutting speed and process instability (greater risk of wire break).
- SPL (short pulse limit): SPL varies from 0 to 31. It is the maximum number of pulses in short circuit (consecutive), before the generator limitations are actuated. This parameter serves for preventing wire breakage which results from bad erosion conditions. Increasing the parameter can lead to a greater risk of wire break and a decrease in erosion time.
- Ton (pulse width): Ton changes from 0 to 32  $\mu$ s. When Ton is increased, it can lead to an increase of the roughness and wire break risk. [31]

#### **4.4 Measuring surface**

After each piece was cut using EDM, deformation on the two cut surfaces was measured on the Alicona. There are different lenses that can be used for scanning. The 10x objective lens shown in Fig. 4.10 has the lowest resolution but it can still provide



one million data points (See Appendix D). The first step of measuring was to find the scanning range of  $X$ ,  $Y$  and  $Z$ . To achieve this, the highest and lowest coordinates along three directions were obtained and Alicona automatically scanned all the points within the block. For the  $Z$  direction, the probe was raised higher at the highest corner and then lowered at the lowest corner to set the  $Z$  range. Every point scanned will be focused at the  $Z$  direction to record the  $Z$  coordinate. The first rough scan took about 10 minutes. It took dozens of pictures and stitched them together (Image filed function). Then the second detailed scan took up to one to two hours. After the second scan was complete, the data was imported as a text file that contains the coordinates of all the data points. The setup for measuring the  $YZ$  cut surface for the displacement along the transverse direction ( $X$  direction) is shown in the Fig. 4.10:

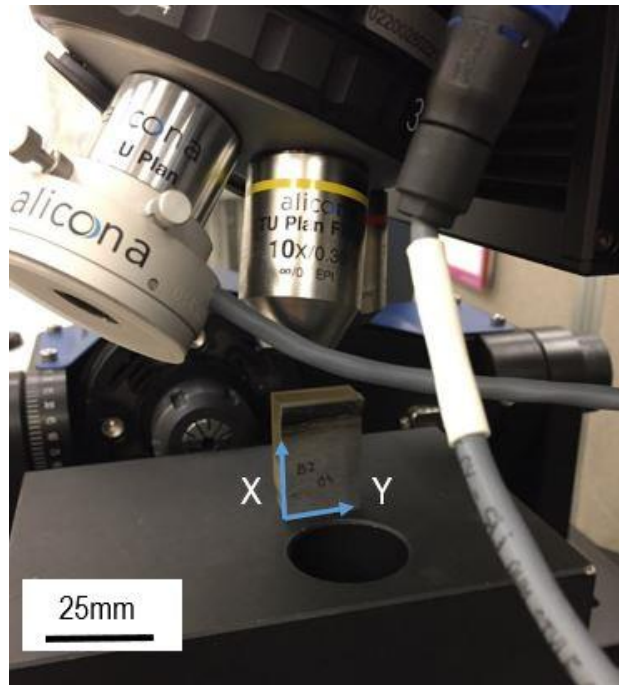


Figure. 4.10 Scanning along X direction (transverse direction).

After the scanning process was complete, the window displayed the following Fig. 4.11 that depicts the surface roughness of the scanned surface:

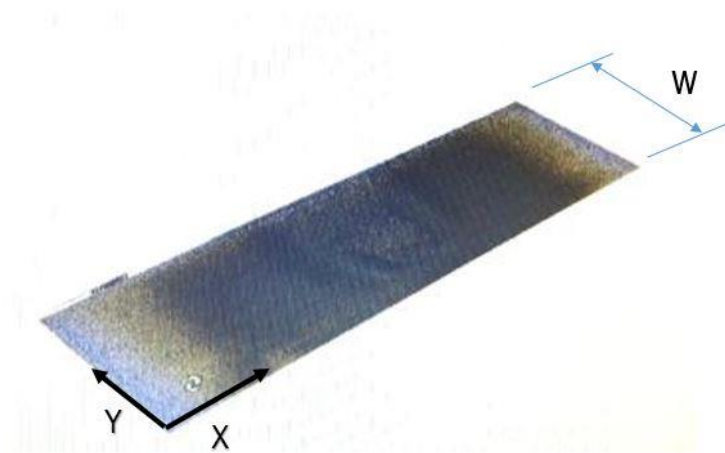


Figure. 4.11. Cut surface contour on XY plane obtained by Alicona.

It is worth noting that the two cut surfaces were both scanned on each piece and later the contours were averaged. This step will be explained in detail in the data processing section. The step by step procedure of using Alicona to scan the surface is documented in Appendix D.

## 5. RESULTS AND DISCUSSION

This chapter presents the residual stress calculation by contour method after the experiments and then residual stress calculation using ANSYS. The residual stress component  $\sigma_x$   $\sigma_y$   $\sigma_z$  calculated by the contour method and submerged arc welding simulation are then compared. The results were extracted at sectional planes at the middle of the specimen for comparison. Also, the calculated residual stress are compared with published data.

### 5.1 Data processing

After the data was obtained using Alicona, it was necessary to process the data and then apply it as boundary condition to the finite element model to calculate the residual stress along different directions. The data file usually contains a large amount of data points and three steps were adopted to process the data. Since the data file was imposed as displacement in ANSYS, the coordinates and amount of points imported into ANSYS should be the same as the nodes on the meshed surface. After the coordinates of points within the meshed surface in the model are known, all the data points gathered by Alicona should be averaged to correspond to the coordinates in ANSYS. However, some outliers or “noise” still exist in the data file. Therefore, smoothing the data file becomes imperative. This was the second step in data processing. After smoothing was done, the last step was to average the two contours on the two corresponding cut surfaces.

### 5.1.1 Average data points

For the scans performed on the cut surfaces, the number of data points gathered range from 140,000 to 280,000. Thus, the first step was to average the data points according to the mesh in the finite element model. This step was done by using the nodes in the meshed model as a triangle center or rectangle center. In this way, all the data points that fall within this area were averaged. Maple software was utilized for this operation. Prior to averaging the data points, tilting operation was carried out. Since Alicona is a 3D optical non-contact measuring technique, there is always a possibility that the surface under scanning is not parallel to the base. Subsequently, it became necessary to tilt the plane so that the  $Z$  value at every data point is referenced from the scanned surface. This plane was uniquely defined by taking three corners node coordinates. Therefore, all the scanned points were then operated based off this plane. The reason for taking the points along the edge is because the residual stress along the edges are zero thus after sectioning, there would not be any displacement. Another issue was that the  $XYZ$  coordinates obtained from Alicona were not recorded based off the edge of the work piece. Therefore, all the coordinates need to be manipulated to fit into a new coordinate system in which the origin was newly defined. The Maple codes for this operation is attached at Appendix C.

To test the validity of the Maple codes, one gage block was put under Alicona in an inclined fashion and the scanned data was put through Maple program and output result showed that Maple can successfully tilt the inclined contour and complete data manipulation from a flat to another flat surface. The details are attached in Appendix E.

### 5.1.2 Data smoothing

This step is also called “noise filtering”. The noise is normally the result of measurement error and the rough cut surface from EDM. The random noise is not caused by the release of the residual stress, and, if not eliminated, will affect the calculated residual stress. There are two steps to filter the noise.

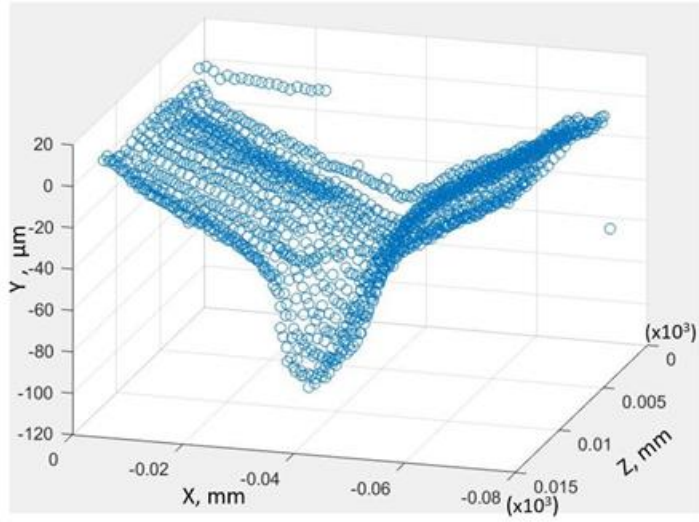
1. The first step is to eliminate obvious outliers. Outliers could result from many factors such as dust settling on the surface during measurement or fluctuations at the edge.
2. The second step is to fit the scanned surface to a smooth surface that eliminates the roughness and noise. The most common and conventional way of fitting is to use Spline Toolbox in Matlab that utilizes bivariate splines [32]. However, this method is not sufficient for the data sample gathered by Alicona because this conventional method cannot take full advantage of the improved spatial resolution of the Alicona. It is fairly difficult to use a single function to fit the complex surface Alicona scans. Therefore, a new method of fitting called Chebyshev polynomials is introduced.

Chebyshev polynomials are a sequence of orthogonal polynomials which can be defined recursively. Chebyshev polynomials are important in approximation theory because the roots of the Chebyshev polynomials of the first kind, which are also called Chebyshev nodes, are used as nodes in polynomial interpolation. Chebyshev polynomials are orthogonal and form a complete base set. They are more suitable for the present problem than, e.g., Fourier expansion because the data we approximate do not

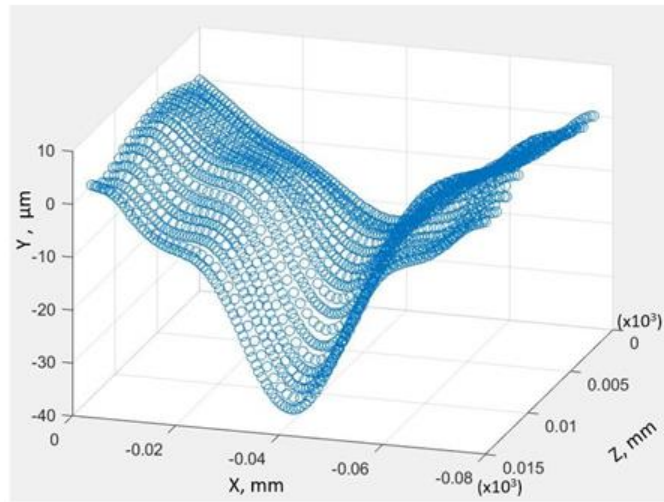
contain spatial oscillations. Since Chebyshev polynomials are orthogonal, the expansion coefficients can be calculated in a straightforward way by a single integration over the area of the sample [33].

### **5.1.3 Average contours**

After the EDM cut, there were two surfaces from each cut piece. Tilting, averaging, and smoothing procedures were performed on the gathered Alicona data of each surface. The last step of data processing is to average the two surfaces (contours). The two scanned surfaces, one from each side of the “cut”, should be aligned to the same coordinate frame such that the material points prior to cutting are coincident on the two surfaces. Averaging contours of the two cut surface will average away all the anti-symmetric errors during the cutting process. These cutting errors stem from either the cut itself wandering or the part moving during cutting as stresses are relaxed and the part deforms. Also, averaging the contours on the two halves can remove effect of shear stress. Fig. 5.1 shows the averaged surface contour prior and after smoothing with Chebyshev polynomials.



(a)



(b)

Figure. 5.1. Surface contour of a specimen after sectioning at  $Y = W/2$  plane (a) Before noise filtering and (b) After filtering.



## 5.2 Stress calculation from experiments

In this section, the residual stresses along three directions will be determined ( $\sigma_x$ ,  $\sigma_y$ ,  $\sigma_z$ , i.e., residual stresses along longitudinal, transverse and thickness directions). The overall steps can be described using the flowchart in Fig 5.2:

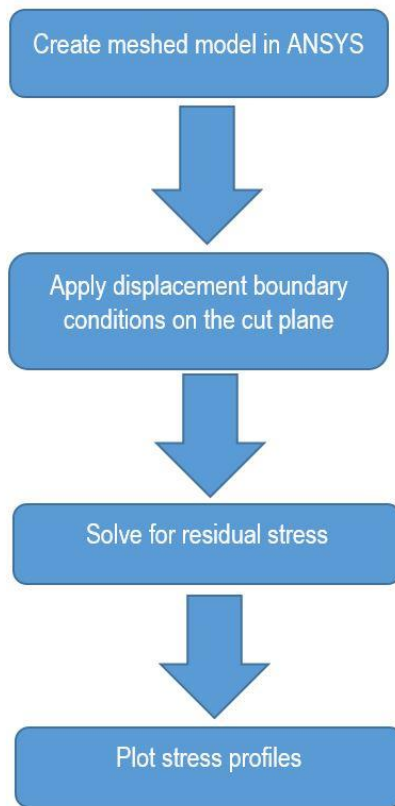


Figure. 5.2. Residual stress calculation flowchart

After the processed data points were obtained, they were applied as the displacement on nodes in finite element model. The number and coordinates of nodes in finite element model depended on the meshing. The finer the mesh, the more nodes

obtained, thus providing a more accurate result. However this can lead to long computational time and at some point the result will converge with no improvement in accuracy no matter how fine the mesh was. APDL coding was used since there were thousands of points to which the displacement constraints were applied. In order to process the data, the coordinates of all the nodes on the sectioned surface were extracted and used as the mesh in the data processing. The underlying issue that occurred with data processing was a possibility of no data points within a certain mesh point. This was because the shape of the piece cannot be guaranteed to be rectangular. There was also a potential for edge fluctuation because of the entry cut. Thus, it was necessary to cut parts of the edges. The procedures for obtaining the residual stress in ANSYS are as follows:

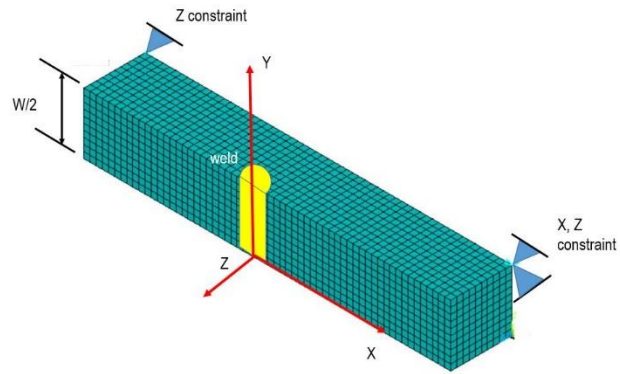
- Step 1: Create finite element model in ANSYS

The first step was to create the finite element model in ANSYS. The APDL coding is attached in APPENDIX B. Fig 5.3 shows the models for obtaining residual stresses along three directions. Displacement constraints were applied on two nodes of the cut surfaces to prevent rigid

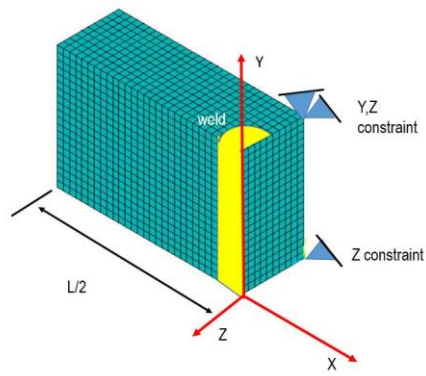
body movement. All the models have the same meshing size of 1.27 mm.

- Step 2: Apply the displacement on the top surface of the model.

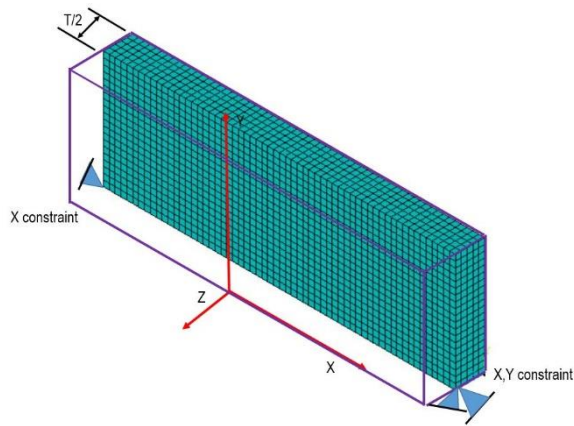
This displacement should be the reverse of what was obtained from Alicona. The Fig. 5.4 shows the effect of adding displacements into the model. Fig. 5.4 (a) shows the  $\sigma_y$  model after the displacement boundary condition was imposed on the  $XZ$  plane at  $Y = W/2$ . Fig. 5.4 (b) shows the  $\sigma_x$  model after the displacement boundary condition was imposed on the  $YZ$  plane at  $X = 0$ . Fig. 5.7 (c) shows  $\sigma_z$  model after the displacement boundary condition was imposed on the  $XY$  plane at  $Z = -L/2$ .



(a)

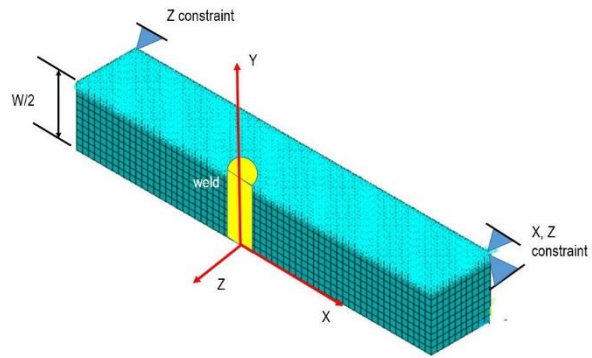


(b)

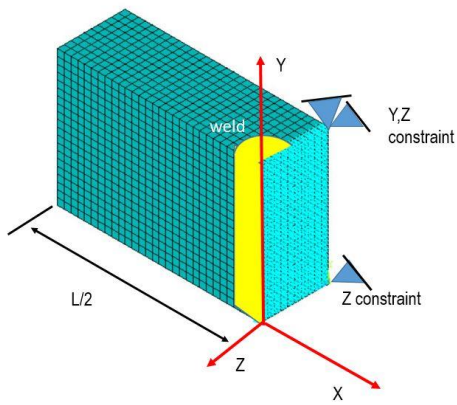


(c)

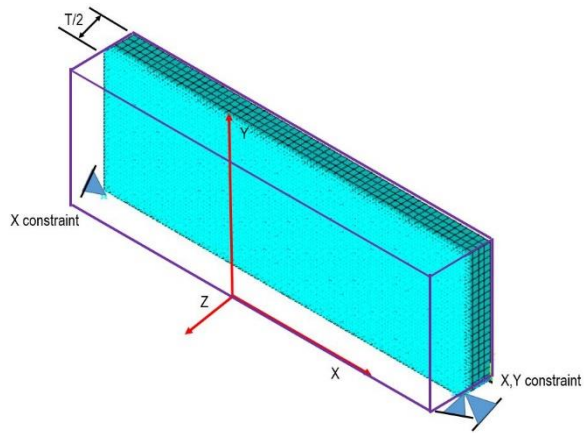
Figure. 5.3. Experiment meshed model for (a)  $\sigma_y$  (b)  $\sigma_x$  (c)  $\sigma_z$



(a)



(b)

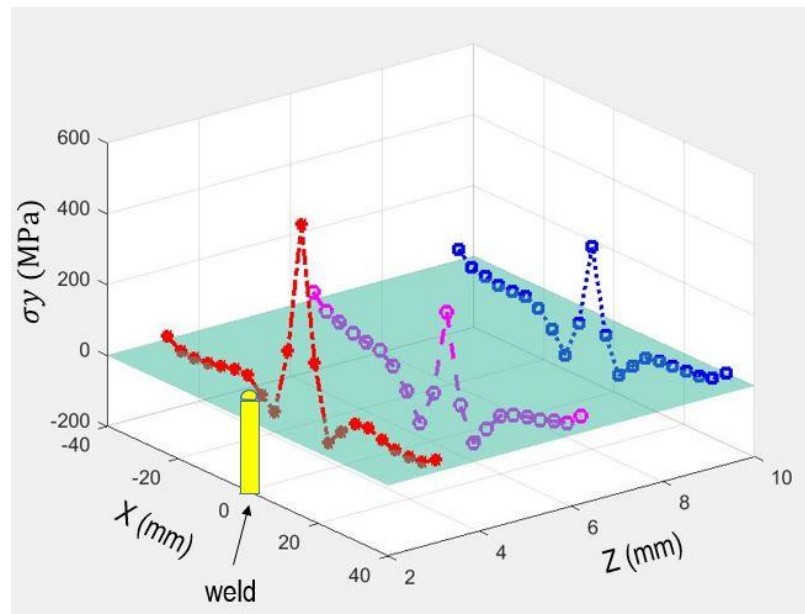


(c)

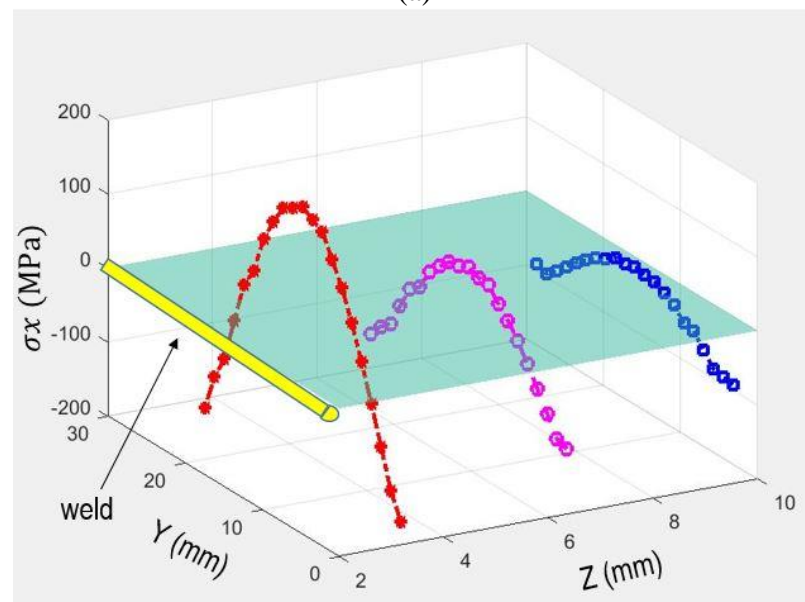
Figure. 5.4. Displacement boundary condition for (a)  $\sigma_y$  (b)  $\sigma_x$  (c)  $\sigma_z$

- Step 3: Solve for residual stress

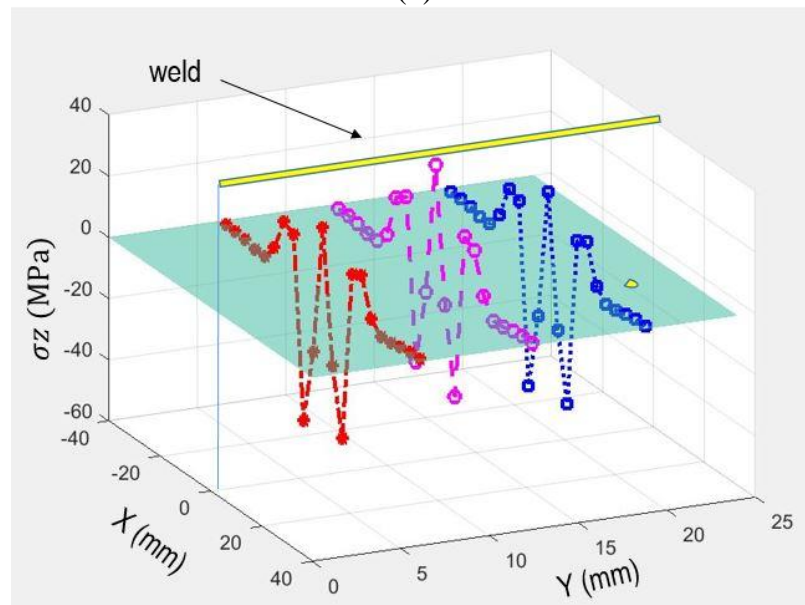
After the boundary condition was applied, residual stresses along the three directions were solved. The longitudinal residual stress profiles at different  $Z$  ( $Z = -T/4, -T/2$  and  $-3T/4$ ) were plotted in Fig. 5.5 (a); The transverse residual stress profiles at different  $Z$  ( $Z = -T/4, -T/2$  and  $-3T/4$ ) were plotted in Fig. 5.5 (b). The along thickness residual stress profiles at different  $Y$  ( $Y = W/4, W/2$  and  $3W/4$ ) were plotted in Fig. 5.5 (c).



(a)



(b)



(c)

Figure 5.5 (a) Residual stress  $\sigma_y$  profiles on XZ-planes at  $Y = W/2$ , along  $Z = -3.17, -6.35,$  and  $-9.51$  mm. (b) Residual stress  $\sigma_x$  profiles on YZ-planes at  $X = 0$ , along  $Z = -3.17, -6.35,$  and  $-9.51$  mm. (c) Residual stress  $\sigma_z$  profiles on XY-planes at  $Z = -T/2$ , along  $Y = 6.35, 12.70,$  and  $19.05$  mm.

### 5.3 Comparison of contour method and simulation

Fig. 5.6 compares the longitudinal residual stress ( $\sigma_y$ ) along centerline obtained by contour method (Fig. 5.5 a) and simulation in Fig. 3.11 ( $XZ$  plane at  $Z = -T/2$ ,  $Y = W/2$ ). Tensile stress is positive in Fig. 5.6.

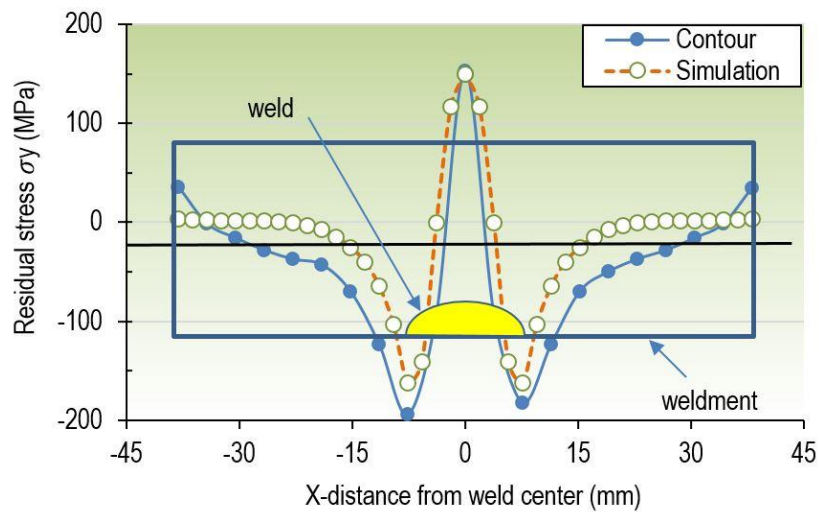


Figure. 5.6. Comparison of longitudinal residual stress ( $\sigma_y$ ) along centerline at  $Z = -T/2$ ,  
 $Y = W/2$

In Fig. 5.6, the range of the data on X axis is from -38.1 mm to 38.1 mm. It is evident that the tensile stress is developed in the weld zone and this tensile stress gradually decreases away from the weld and it turned out to be a compressive stress. This is because when the weld zone cools down, its contraction is constrained by the neighborhood of weld zone, resulting in the tensile stress. The peak value of the tensile



stress obtained in simulations was in a good agreement with the measured tensile stress.

The reasons for some discrepancies towards the end were twofold:

- a. The “bulge” error that occurred during the EDM process. Since cutting process made a cut of constant kerf width  $K$  in the reference frame and as the process proceeds, the stresses relaxed and material at the tip of the cut deformed while the cut still remained to be  $K$ . Thus width of the cut had been reduced when measured relative to the original state of the body.
- b. The entry cut caused lots of fluctuations at the edge of the scanned profile. Parts of the data around the parameter had to be cut to gain a more accurate result. Since the stress approaching the edge was almost 0, these irregularities should be removed in the data fitting process.

The longitudinal residual stress ( $\sigma_y$ ) was found to be tensile at weld center with a magnitude of 150 MPa and turned into compressive residual stress (around 160 MPa) farther away from the weld.

In Fig. 5.7, the transverse residual stresses ( $\sigma_x$ ) obtained in simulations (Fig. 3.8) and in the contour method (Fig. 5.5 b) along centerline ( $YZ$  plane at  $Z = -T/2$ ,  $X = 0$ ) are compared. Also, another repeatability test from contour method is also incorporated in the comparison. Tensile stress is positive.

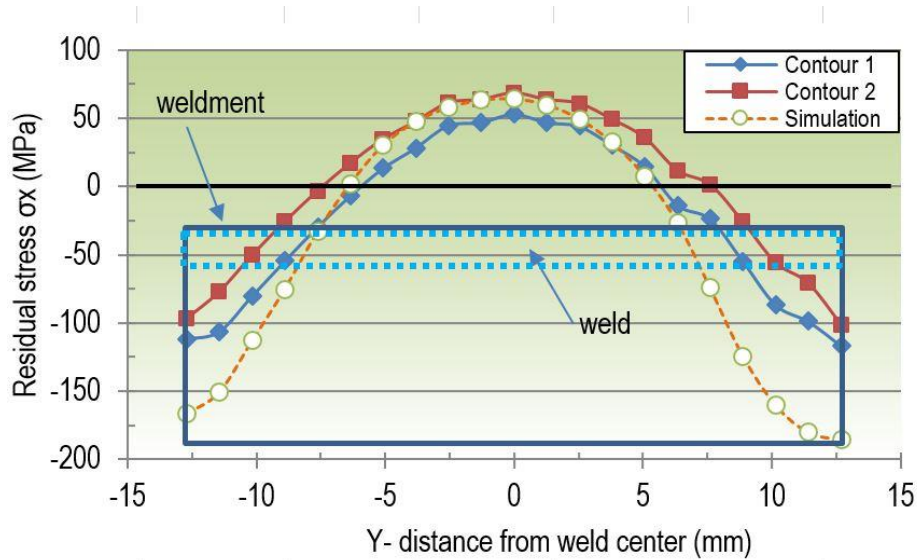


Figure. 5.7. Comparison of transverse residual stress ( $\sigma_x$ ) along centerline at  $Z = -T/2$ ,  $X = 0$

It can be seen from Fig. 5.7 that the tensile stress exists in the middle of the weld and compressive stress exists towards the end. The range of the data in the  $X$  axis is from 0 to 25.4 mm. The fluctuations occur at the two ends. The experimental stresses profile agrees within 10% accuracy with simulations towards the middle.

To confirm the repeatability of the method, a second sample was analyzed using the same parameters for the transverse residual stress (Contour 1 and contour 2 in Fig. 5.7). The results obtained in both experiments match each other well with an overall discrepancy of less than 18%.

The transverse residual stress variation ( $\sigma_x$ ) shows a tensile stress of around 55 MPa at middle weld bead and turns into compressive towards the two ends of the weld

bead with a value of 150 MPa. The trend is due to non – uniform thermal expansion during the heating phase and shrinkage during cooling phase. The compressive residual stress at two ends develops to balance out the tensile stress at the center.

Finally, Fig. 5.8 shows the residual stress in thickness direction ( $\sigma_z$ ) along centerline ( $XY$  plane at  $Z = -T/2, Y = W/2$ ) obtained from contour method (Fig. 5.5 c) and simulation (Fig. 3.13). Tensile stress is positive.

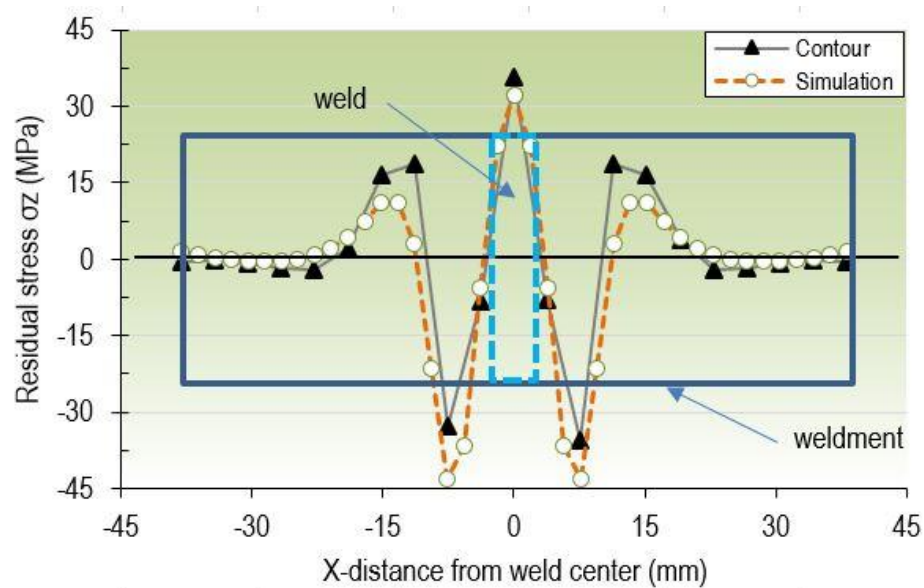


Figure. 5.8. Comparison of residual stress ( $\sigma_z$ ) along centerline at  $Z = -T/2, Y = W/2$

The range of the data in  $X$  axis is from -38.1 mm to 38.1 mm. It can be seen from the plot above that the magnitude of the residual stress along thickness direction is around 75% lower than along the longitudinal (150 MPa from longitudinal direction versus 35 MPa from long thickness direction). The experimental stresses profile overall

matches with simulation and the highest tensile residual stresses from experiment and simulation coincide well with an accuracy of within 9%. (36 MPa from experiment versus 32 MPa from simulation).

For residual stress in thickness direction ( $\sigma_z$ ) the tensile stress is maximum at middle weld and turns into compressive as it moves towards the two ends, following by transitioning into tensile again as it moves closer to the two ends. The reason why tensile stress develops in the center is because the middle (close to weld) cools down first compared to the surrounding material and the cooling is restricted by the neighbourhood, thus developing tensile stress.

#### **5.4 Compare with published data**

The residual stress profiles are similar to those in published literature. We compare the trend and shape of residual stress profiles rather than the magnitudes and slopes of residual stress plots, since researchers used different welding techniques, weldment materials and sizes, different clamping techniques that resulting in different boundary conditions, and they applied different welding parameters in their respective experiments.

From Fig. 5.6, the longitudinal residual stress ( $\sigma_y$ ) was tensile at weld center with a magnitude of 150 MPa and turned into compressive residual stress (around 160 MPa) farther away from the weld. This trend agreed well with the published results by Murugan et al. [18] which indicated the tensile residual in a *T*-joint stresses reached 400 MPa at the center and gradually decreased in the transverse direction away from weld

center line and became compressive residual stresses (up to 270 MPa) towards the edge of the plate. This is shown in Fig. 5.9. The magnitude between two studies varied greatly because the welding parameters used in two experiments were different. These authors used gas metal arc welding (GMAW) with an arc voltage of 30 V, welding current of 210 A and welding speed of 4.467 mm/sec to weld two pieces into a *T* joint. The two pieces had dimension of  $210 \times 100 \times 5$  mm and  $210 \times 50 \times 5$  mm. Finite element simulation was also adopted to compare with contour method; the researchers found that the peak value of tensile residual stresses obtained by the simulation was in good agreement with the peak value obtained by the contour method.

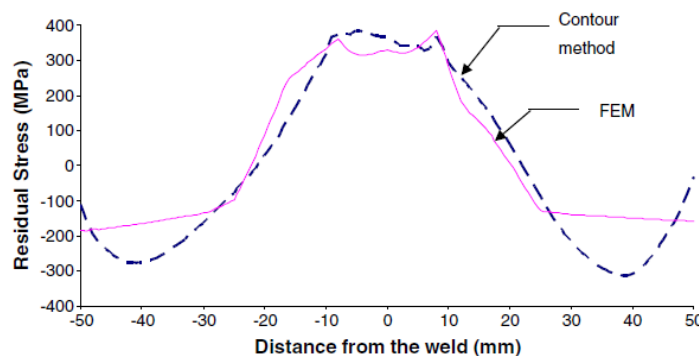


Figure. 5.9. Distribution of longitudinal residual stress. Reprinted from [19]

The transverse residual stress ( $\sigma_x$ ) in Fig. 5.7 showed a tensile stress of around 55 MPa at middle weld bead and turned into compressive towards the two ends of the weld bead with a value of 150 MPa. This trend was similar to the published data by Thorat et al. [34] shown in Fig. 5.10, in which he found that, for residual stresses

distribution in a butt weld, the middle weld bead was in tension and the magnitude of equaled to 30 MPa whereas the ends of the weld were in compression with a value of 100 MPa. These authors used GMAW to butt weld two  $300 \times 100 \times 5$  mm pieces with a welding current of 110 A, voltage 20 V and welding speed of 5 mm/s.

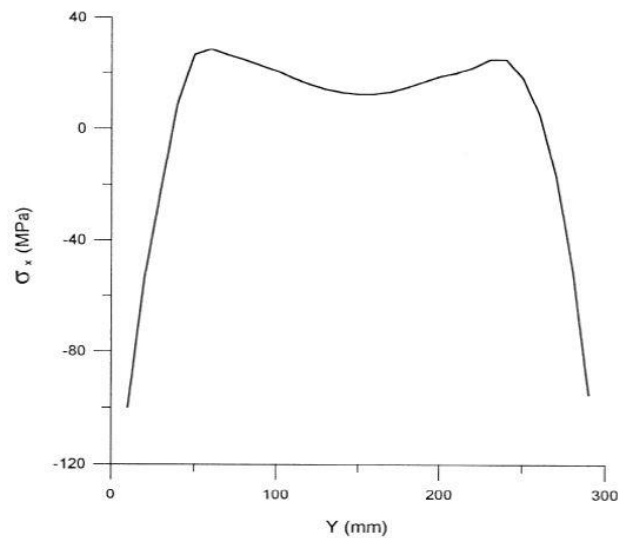


Figure. 5.10. Distribution of transverse residual stress. Reprinted from [34]

Fig. 5.8 shows that, for residual stress in the thickness direction ( $\sigma_z$ ), the tensile stress was maximum at middle weld and turned into compressive as it moved towards the two ends, following by transitioning into tensile again as it moved closer to the two ends. This trend aligned with the residual stress variation along thickness direction in a butt-welded A36 steel plate with a bead width of 8mm and a bead height of 0.3mm by Ogawa et al. [35]. The plate length, thickness and width are 120mm, 10mm and 60mm,

respectively. Fig 5.11 shows the residual stress profiles along three directions, including along thickness direction. It is clear that the stress is tensile close to the middle of the weld and turns compressive towards two ends, following by turning into around tensile/zero at two ends. It can also be observed that the magnitude of the residual stress along thickness direction is significantly lower than other two directions.

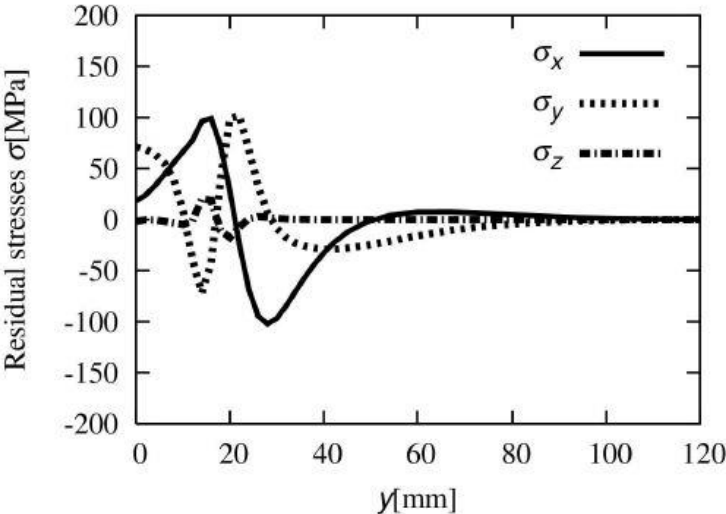


Figure. 5.11. Exact residual stress distributions in three directions. Reprinted from [35]

## 6. CONCLUSIONS AND RECOMMENDATION

Contour method and finite element analysis (FEA) were used to compute and compare the resulting residual stress after welding. This study showed:

- 1) Contour method is a valuable method to show through-thickness residual stress distribution in different directions.
- 2) A surface profile measured by precision optical technique provides more accurate data than mechanical approach using a coordinate measuring machine.
- 3) Tensile residual stresses at the weld are confirmed, and agreed, by both contour method and FEA. The residual stress  $\sigma_y$  along the welding direction has the highest magnitude of 150 MPa. This peak value diminishes at location away from the weld.

Additional steps would be implemented in future investigations:

- a) Although the repeatability of  $\sigma_x$  was shown, additional weldments for repeatability study in  $Y$  and  $Z$  directions would complete the study.
- b) A weld bead was deposited on top of a weldment in this study. Applying the contour technique on a butt joint would give invaluable results.
- c) Contour technique can be used to find optimized welding parameters.



## REFERENCES

- [1] V. Trufyakov, P. Mikheev, Y. Kudryavtsev. 1999. Fatigue strength of welded structures. London: Harwood Academic, p. 100.
- [2] P. J. Withers, H. K. D. H. Bhadeshia. 2001. Residual stress part 2 - nature and origins. *Materials Science and Technology*, Vol. 17, p. 366-375.
- [3] W. Borland, 1997. Residual stress measurement -Methods, limitations and significance. *Quality Control and Assurance in Advanced Surface Engineering*, Inst of Materials, p. 113-125.
- [4] S. Kou. 2003. *Welding Metallurgy*. Wiley-Interscience Hoboken Publishing. 2nd Edition. New Jersey.
- [5] J. F. Lancaster. 1999. *Metallurgy of Welding*, Abington Publishing, 6th edition, England.
- [6] W. E. Littmann. 1964. Measurement and significance of residual macro stress in steel. *SAE 793A, Proc. of the Automatic Eng. Cong.* Vol. 6, p. 4183-4188.
- [7] C. L. Jenney, A. O. Brien 2001. *AWS handbook*. American Welding Society Publishing. *Residual Stress and Distortion*. 9th edition. Vol. 1. Miami.
- [8] [https://en.wikipedia.org/wiki/Submerged\\_arc\\_welding](https://en.wikipedia.org/wiki/Submerged_arc_welding).
- [9] <https://www.twi-global.com/technical-knowledge/job-knowledge/submerged-arc-welding-process-005/>
- [10] N. S. Rossini, M. Dassisti, K.Y. Benyounis, A.G. Olabi. 2012. Methods of measuring residual stresses in components. *Materials and Design*. Vol. 35, p. 572–588.

- [11] C. Lachmann, T. N. Pagel, H. Wohlfahrt. 1999. Non-destructive characterization of fatigue processes in cyclically loaded welded joints by the Barkhausen noise method. Stanford University: 2nd International Workshop on Structural Health Monitoring.
- [12] H. Bueckner, 1958. The propagation of cracks and the energy of elastic deformation. Transactions of the American Society of Mechanical Engineers. Vol. 80, p. 1225-1230.
- [13] W. Cheng, I. Finnie, M. Gremaud, M. B. Prime. 1994. Measurement of near-surface residual stresses using electric-discharge wire machining. Journal of Engineering Materials and Technology. Vol. 116, p. 1-7.
- [14] M. B. Prime, A. L. Kastengren. 2011. The contour method cutting assumption: error minimization and correction. Experimental and Applied Mechanics. Conference Proceedings of the Society for Experimental Mechanics Series. Vol. 6, p. 233-250.
- [15] M. B. Prime, M. R. Hill, A. T. DeWald, R. J. Sebring, V. R. Dave, M. J. Cola. 2003. Residual stress mapping in welds using the contour method. Proceedings of the 6th International Conference. ASM International. P. 891-896
- [16] A. G. Olabi, M. S. J. Hashmi. 1996. Stress relief procedures for low carbon steel (1020) welded components. J Mater Process Technology. Vol. 56, p. 552-562.
- [17] P. Martinson, S. Daneshpour, M. Kocak, S. Riekehr, P. Staron. 2009. Residual stress analysis of laser spot welding of steel sheets. Materials and Design. Vol. 30, p. 3351-3359.
- [18] N. Murugan, R. Narayanan. 2009. Finite element simulation of residual stresses and their measurement by contour method. Materials and Design. Vol. 30, p. 2067-2071.

- [19] A. E. Hami, B. Radi. 2017. Fluid-Structure Interactions and Uncertainties: Ansys and Fluent Tools. Wiley-ISTE publishing. 1st edition.
- [20] J. N. DuPont, A. R. Marder. 1995. Thermal efficiency of arc welding processes. Welding Journal. Vol. 74, p. 406-416.
- [21] D. V. Kiranand, S. J. Na. 2014. Numerical studies on submerged arc welding process. Journal of Welding and Joining. Vol. 32, p. 1-9.
- [22] Lincoln Electric - Submerged Arc Welding handbook
- [23] J. Goldak, A. Chakravarti, M. Bibby. 1984. A new finite element model for welding heat sources. Metallurgical Transactions B. Vol. 15, Issue 2, p. 299–305.
- [24] D. Stamenković, I. Vasović. 2009. Finite element analysis of residual stress in butt welding two similar plates. Scientific Technical Review. Vol. LIX, No.1.
- [25] [http://www.ansys.stuba.sk/html/elem\\_55/EBooktoc.htm](http://www.ansys.stuba.sk/html/elem_55/EBooktoc.htm).
- [26] [https://www.sharcnet.ca/Software/Ansys/16.2.3/enus/help/wb\\_msh/msh\\_book\\_wb.html](https://www.sharcnet.ca/Software/Ansys/16.2.3/enus/help/wb_msh/msh_book_wb.html).
- [27] [https://www.sharcnet.ca/Software/Ansys/16.2.3/en-us/help/cfx\\_mod/i1313549.html](https://www.sharcnet.ca/Software/Ansys/16.2.3/en-us/help/cfx_mod/i1313549.html)
- [28] M. S. Choobi, M. Haghpanahi and M. Sedighi, 2010. Investigation of the effect of clamping on residual stresses and distortions in butt-welded plates. Transaction B: Mechanical Engineering. Vol. 17, No. 5, pp. 387-394
- [29] [https://www.sharcnet.ca/Software/Ansys/16.2.3/en/ us/help/ans\\_bas/Hlp\\_G\\_BasTOC.html](https://www.sharcnet.ca/Software/Ansys/16.2.3/en/us/help/ans_bas/Hlp_G_BasTOC.html)
- [30] <https://www.azom.com/article.aspx?ArticleID=6117>

- [31] C. Sommer, S. Sommer, 2005. Complete EDM Handbook. Advance Publishing, Incorporated.
- [32] M. B. Prime, R. J. Sebring, J. M. Edwards, D. J. Hughes, P. J. Webster. 2004. Laser surface contouring and spline data-smoothing for residual stress measurement. *Experimental Mechanics*. Vol. 44, p. 176-184
- [33] S. M. Dardery, M. M. Allan. 2014. Chebyshev polynomials for solving a class of singular integral equations. *Applied Mathematics*. Vol. 5, p. 753-764.
- [34] S. R. Thorat, Y. R. Kharde, K. C. Bhosale, S .B. Kharde. Effect of welding conditions on residual stresses and heat source distribution on temperature variations on butt welds: A review. *International Journal of Engineering Research and Applications (IJERA)* ISSN: 2248-9622. Vol. 3, p.1434-1439.
- [35] M. Ogawa, K. Hodogaya, S. Yokohama, K. Kanagawa. Three-dimensional welding residual stresses evaluation based on the eigen-strain methodology via X-ray measurements at the surface. ICCM2014, 28-30<sup>th</sup> July, Cambridge, England. Vol. 3. Issue 4.

## APPENDIX A

### ANSYS PARAMETRIC DESIGN LANGUAGE (APDL) CODING FOR SUBMERGED ARC WELDING SIMULATION

This appendix contains the APDL coding for carrying out thermal analysis and stress analysis for submerged arc welding. The following are the table lists:

Table A1: APDL commands for defining material properties.

Table A2: APDL commands for building 3-D model and meshing.

Table A3: APDL commands for thermal analysis.

Table A4: APDL commands for stress analysis.

Table A1: Define material properties		
Line #	Command	Comment
1	/PREP7	! Go to Preprocessing
2	MPTEMP,1,0,100,200,300,400,600	! Set temperature
3	MPTEMP,7,800,1200,1300,1500	
4	MPDATA,KXX,1,1,14.6,15.1,16.1,17.9,18.0,20.8	! Set thermal conductivity
5	MPDATA,KXX,1,7,23.9,32.2,33.7,120	

6	MPDATA,DENS,1,1,7900,7880,7830,7790,7750,7660	! Set density at different temperature
7	MPDATA,DENS,1,7,7560,7370,7320,7320	
8	MPDATA,C,1,1,462,496,512,525,540,577	! Set specific heat at different temperature
9	MPDATA,C,1,7,604,676,692,935	
10	MPDATA,EX,1,1,1.985e11,1.93e11,1.85e11,1.76e11,1.67e11,1.59e11	! Set modulus of elasticity
11	MPDATA,EX,1,7,1.51e11,6e10,2e10,1e10	
12	MPDATA,PRXY,1,1,0.294,0.295,0.301,0.310,0.318,0.326	! Set Poisson's ratio
13	MPDATA,PRXY,1,7,0.333,0.339,0.342,0.388	
14	UIMP,1,REFT,,,20	! Set the reference temperature to be 20° C
15	TB,BISO,1,6,2,	! Define yield stress at six
16	TBTEMP,0	

17	TBDATA,,265e6,0,,,	different temperatures
18	TBTEMP,100	
19	TBDATA,,218e6,0,,,	
20	TBTEMP,300	
21	TBDATA,,170E6,0,,,	
22	TBTEMP,600	
23	TBDATA,,149E6,0,,,	
24	TBTEMP,1200	
25	TBDATA,,25E6,0,,,	
26	TBTEMP,1500	
27	TBDATA,,10E6,0,,,	

Table A2: Build 3-D model and create mesh		
Line #	Command	Comment
1	/PREP7	! Go to preprocessing
2	/UNITS,Si	! Set Unit
3	L=0.0254	! Weldment length
4	W=0.0762	! Weldment width
5	H=1.27E-2	! Weldment height
6	ET,1,PLANE55	! Define 2-D element type
7	ET,2,SOLID70	! Define 3-D element type
8	K,1,0,0,0	! Define key points by coordinates
9	K,2,0,L,0	
10	K,3,-W/2*0.15,L,0	
11	K,4,-W/2*0.3,L,0	
12	K,5,-W/2*0.5,L,0	
13	K,6,-W/2,L,0	
14	K,7,-W/2,0,0	
15	K,8,-W/2*0.5,0,0	
16	K,9,-W/2*0.3,0,0	
17	K,10,-W/2*0.15,0,0	
18	K,11,0,0,H	



19	A,1,2,3,10	! Define face by key points. Area 1 is the closest to the weld
20	A,10,3,4,9	! Area 2 is next to area 1 but further
21	A,9,4,5,8	! Area 3 is next to area 1 but even further
22	A,8,5,6,7	! Area 4 is the furthest from the weld
23	ESIZE,0.0008	! Mesh different area with different accuracy, finer close to weld bead, coarser far from weld Default element edge length on surface boundaries to be 0.0008
24	AMESH,1	! Mesh area 1 (the finest mesh) with the size defined in line 23
25	ESIZE,0.0012	! Default element edge length on surface boundaries to be 0.0012
26	AMESH,2	! Mesh area 2 with the size defined above
27	ESIZE,0.0025	! Default element edge length on surface boundaries to be 0.0025
28	AMESH,3	! Mesh area 3 with the size defined above

29	ESIZE,0.005	! Default element edge length on surface boundaries to be 0.005
30	AMESH,4	! Mesh area 4 (the most coarse mesh) with the size defined above
31	TYPE, 2	! Switch element type from 2D PLANE55 to 3D
32	SOLID70	
33	EXTOPT,ESIZE, 6,0,	! Volume will be divided into 6 part during extrusion
34	EXTOPT,ATTR,1,0,0	! 1,0,0 means respectively: Sets volume elements to use material attributes of the pattern area elements, Sets volume elements to use current REAL command settings, Sets volume elements to use current ESYS command settings.
35	REAL,_Z4	
36	ESYS,0	! Set coordinate system
37	VOFFST,1,H, ,	! Extrude area 1 for H inches, H is the weldment height

38	VOFFST,2,H, ,	! Extrude area 2 for H inches, H is the weldment height
39	VOFFST,3,H, ,	! Extrude area 3 for H inches, H is the weldment height
40	VOFFST,4,H, ,	! Extrude area 4 for H inches, H is the weldment height
41	ELOT	! Produce element display
42	NUMMRG,ALL, , , ,LOW	! Merge all the items due to extrusion of different faces

Table A3: Thermal analysis		
Line #	Command	Comment
1	/PREP7	! Go to preprocessing
2	V=0.01267	! Set welding speed
3	YITA=0.7	! Set welding thermal efficiency
4	R=0.007	! Effective heat arc radius
5	Q=U*I*YITA	! Heat input
6	Qm=3/3.1415/R**2*Q	! Center best spot heating flux
7	/SOL	! Go to solution, start transient thermal analysis
8	ANTYPE,4	! Perform transient analysis
9	TRNOPT,FULL	! Set solution method as full
10	LUMPM,0	! Do not use lumped mass approximation
11	*DEL,_FNCNAME	! Start defining Gaussian heat source function
12	*DEL,_FNCMTID	
13	*DEL,_FNC_C1	
14	*DEL,_FNC_C2	
15	*DEL,_FNC_C3	
16	*DEL,_FNCCSYS	
17	*SET,_FNCNAME,'GAOSI'	! Set function name to be GAOSI

18	*DIM,_FNC_C1,,1	! Defines an array parameter and its dimensions.
19	*DIM,_FNC_C2,,1	
20	*DIM,_FNC_C3,,1	
21	*SET,_FNC_C1(1),QM	! Assign value QM to FNC_C1.
22	*SET,_FNC_C2(1),V	! Assign value V to FNC_C2
23	*SET,_FNC_C3(1),R	! Assign value R to FNC_C3.
24	*SET,_FNCCSYS,0	! INPUT,HANJIE.func,,,1
25	*DIM,%_FNCNAME%,TABLE,6 ,19,1,,,,%_FNCCSYS%	! Begin of equation: $Q_m \exp(-3 * (X^2 + (Y - V * TIME)^2) / R^2)$
26	*SET,%_FNCNAME%(0,0,1), 0.0, -999	
27	*SET,%_FNCNAME%(2,0,1), 0.0	
28	*SET,%_FNCNAME%(3,0,1), % _FNC_C1(1)%	
29	*SET,%_FNCNAME%(4,0,1), % _FNC_C2(1)%	
30	*SET,%_FNCNAME%(5,0,1), % _FNC_C3(1)%	
31	*SET,%_FNCNAME%(6,0,1), 0.0	

32	*SET,%_FNCNAME%(0,1,1), 1.0, -1, 0, 0, 0, 0, 0	! The commands for defining equation $Q_m \cdot \exp(-3 \cdot (X)^2 + (Y) - V \cdot (TIME)^2 / R^2)$ seem erratic and convoluted. To obtain this code, we need to use APDL interface to first type in function (Parameter-> function) and then save it as *func file. If we open this file in notepad. We will obtain the commands on the left.
33	*SET,%_FNCNAME%(0,2,1), 0.0, -2, 0, 1, 0, 0, -1	
34	*SET,%_FNCNAME%(0,3,1), 0, -3, 0, 1, -1, 2, -2	
35	*SET,%_FNCNAME%(0,4,1), 0.0, -1, 0, 3, 0, 0, -3	
36	*SET,%_FNCNAME%(0,5,1), 0.0, -2, 0, 1, -3, 3, -1	
37	*SET,%_FNCNAME%(0,6,1), 0.0, -1, 0, 2, 0, 0, 2	
38	*SET,%_FNCNAME%(0,7,1), 0.0, -3, 0, 1, 2, 17, -1	
39	*SET,%_FNCNAME%(0,8,1), 0.0, -1, 0, 1, 18, 3, 1	
40	*SET,%_FNCNAME%(0,9,1), 0.0, -4, 0, 1, 3, 2, -1	
41	*SET,%_FNCNAME%(0,10,1), 0.0, -1, 0, 2, 0, 0, -4	
42	*SET,%_FNCNAME%(0,11,1), 0.0, -5, 0, 1, -4, 17, -1	

43	*SET,%_FNCNAME%(0,12,1), 0.0, -1, 0, 1, -3, 1, -5	
44	*SET,%_FNCNAME%(0,13,1), 0.0, -3, 0, 1, -2, 3, -1	
45	*SET,%_FNCNAME%(0,14,1), 0.0, -1, 0, 2, 0, 0, 19	
46	*SET,%_FNCNAME%(0,15,1), 0.0, -2, 0, 1, 19, 17, -1	
47	*SET,%_FNCNAME%(0,16,1), 0.0, -1, 0, 1, -3, 4, -2	
48	*SET,%_FNCNAME%(0,17,1), 0.0, -1, 7, 1, -1, 0, 0	
49	*SET,%_FNCNAME%(0,18,1), 0.0, -2, 0, 1, 17, 3, -1	
50	*SET,%_FNCNAME%(0,19,1), 0.0, 99, 0, 1, -2, 0, 0	
51	TUNIF,20,	! Define the initial temperature
52	SFA,15,1,CONV,30,20	! Define convective heat transfer boundary. 15 is the area number
53	SFA,20,1,CONV,30,20	! 30 W/(m <sup>2</sup> K) is the film coefficient, 20 ° C is bulk temperature

54	SFA,9,1,CONV,30,20	! All the areas are imposed with convective boundary condition except from area A5, A6 and A10.
55	SFA,14,1,CONV,30,20	
56	SFA,19,1,CONV,30,20	
57	SFA,24,1,CONV,30,20	
58	SFA,23,1,CONV,30,20	
59	SFA,7,1,CONV,30,20	
60	SFA,12,1,CONV,30,20	
61	SFA,17,1,CONV,30,20	
62	SFA,22,1,CONV,30,20	
63	SFA,1,1,CONV,30,20	
64	SFA,2,1,CONV,30,20	
65	SFA,3,1,CONV,30,20	
66	SFA,4,1,CONV,30,20	
67	SFA,5,1,HFLUX, %GAOSI%	! Now apply gaussian heat source for area A5 and A10
68	SFA,10,1,HFLUX, %GAOSI%	
69	/SOL	! Go to solution
79	OUTRES,ALL,ALL,	! Write each solution results item for every substep to database
80	TIME,L/V	! Setting the computation time
81	AUTOTS, AUTO (-1)	! Set Automatic time stepping key
82	NSUBST,50,50,50	! 50 sub steps are taken in this load step



83	KBC,0	! Define the way the load is imposed, ramped
84	TSRES,ERASE	! To clear the array parameter specification
85	LSWRITE,1,	! Write load file 1
86	TIME,10	! Set the computation time to be 10 seconds, 10 seconds include the 2 second from previous step since there is 80 sub steps taken thus the step size should be 0.1s
87	AUTOTS,AUTO	! Set Automatic time stepping key
88	NSUBST,80,80,80	! 80 sub steps are taken in this load step
89	KBC,0	
90	TSRES,ERASE	
91	LSWRITE,2,	! Write load file 1
92	TIME,40	! Setting the computation time to be 40 seconds
93	AUTOTS,AUTO (1)	
94	NSUBST,60,60,60	! 60 sub steps are taken in this load step, sub step time size is 0.5s

95	KBC,0 TSRES,ERASE	
96	LSWRITE,3,	! Write load file 3
97	TIME,190	! Setting the computation time to be 190 seconds
98	AUTOTS,AUTO (1)	
99	NSUBST,100,100,100	! 100 sub steps are taken in this load step, sub step time size is 1.9s
100	KBC,0	
101	TSRES,ERASE	
102	LSWRITE,4,	! Write load file 3
103	LSSOLVE,1,4,1,	! Start solving for temperature field

Table A4: Stress analysis		
Line #	Command	Comment
1	/PREP7	
2	ETCHG,TTS	! Change element type from thermal (solid70) to structural (solid185)
3	/SOL	! Go to solution
4	ANTYPE,4	! Perform a transient analysis
5	TRNOPT,FULL	! Use full method (default) for transient analysis
6	LUMPM,0	! Specify element-dependent default mass matrix formulation
7	NLGEOM,1	! Large deformation analysis on
8	NROPT,FULL, ,OFF	! Use full Newton-Raphson. Do not use adaptive descent (OFF).
9	TREF,20,	! Define thermal stress calculation reference temperature
10	/SOL	
11	DA,6,SYMM	! Set symmetrical displacement constraints
12	DK,1,UY,0,,,UZ	
13	DK,2,UZ,0	! Setting displacement constraints

14	DA,6,UX,0	
15	DL,44,UY,0	
16	*DO,I,1,50	! Apply temperature history generated by thermal analysis through *Do loop
17	LDREAD,TEMP,,0.04*I, , 'weldingstress', 'rth', ''	! Read the results of thermal analysis
18	OUTRES,ALL,ALL,	
19	TIME,0.04*I	
20	DELTIM,0.04,0.04,0.04,1	! Define time step
21	SOLVE	
22	*ENDDO	
23	*DO,I,1,80	! 2 seconds are from the first loop, 0.1s is the time step corresponding to previous thermal analysis
24	LDREAD,TEMP,,2+I*0.1, , 'weldingstress', 'rth', ''	
25	OUTRES,ALL,ALL,	
26	TIME,2+I*0.1	
27	DELTIM,0.1,0.1,0.1,1	
28	SOLVE	
29	*ENDDO	
30	*DO,I,1,60	
31		

	LDREAD,TEMP,,,10+I*0.5,,'wel	
32	dingstress','rth',''	
33	OUTRES,ALL,ALL,	
34	TIME,10+I*0.5	
35	DELTIM,0.5,0.5,0.5,1	
36	SOLVE	
37	*ENDDO	
38	*DO,I,1,100	
	LDREAD,TEMP,,,40+1.5*I,,'wel	
39	dingstress','rth',''	
40	OUTRES,ALL,ALL,	
41	TIME,40+1.5*I	
42	DELTIM,1.5,1.5,1.5,1	
43	SOLVE	
	*ENDDO	

## APPENDIX B

### ANSYS APDL CODING AND GUI GUIDE FOR RESIDUAL STRESS

#### SIMULATION FROM EXPERIMENTS

This Appendix contains the GUI guide for obtaining residual stress simulation from experiments and the APDL coding for building models in three orthogonal directions.

The following is the table list in Appendix B.

Table B1: GUI guide for obtaining residual stress profile in ANSYS

Table B2: APDL code for building a model for stress along *Y* direction

Table B3: APDL code for building a model for stress along *X* direction

Table B4: APDL code for building a model for stress along *Z* direction

Table B1: GUI guide for obtaining residual stress profile in ANSYS	
GUI Guide	Purpose
General Postproc -> Path Operation-> Define Path-> By nodes (or by location) (write down name, number of data sets, number of division) -> Map Onto Path (under Path Operation)-> (pick dataset) ->plot path item (under Path Operation)->On graph (choose item)->obtain result	Obtain stress along a defined line

<p>Workplane-&gt; offset WP by Increments -&gt; X Y Z offset; Degrees  XY、YZ、ZX Angles-&gt; PlotCtrls-&gt; Style-&gt; Hidden Line Options -&gt;  Type of Plot (Section); Cutting Plane is (Working plane)</p>	<p>Move working plane for  longitudinal residual  stress</p>
<p>PlotCtrls-&gt; Style-&gt; Colors-&gt; Reverse video (this step change the  background color into white) -&gt; plotctrls-&gt; style-&gt; Hidden Line  options-&gt; apply-&gt; Plotctrls-&gt; Capture Image-&gt;save as (using custom  aspect ratio)</p>	<p>Plot sectioned graph.</p>

Table B2: Build a model for stress along Y direction		
Line #	Command	Comment
1	/FILENAME, SIGMAY	
2	/PREP7	! Weldments defined parameters
3	L=0.0254	! Weldment length
4	W=0.0762	! Weldment width
5	H=1.27E-2	! Weldment height
6	ET,1,SOLID186	
7	MP,EX,1, 2E11	! Young's Modulus
8	MP,PRXY,1,0.3	! Poisson's ratio
9	K,2,0,0,H	
10	K,6,0,L/2,H	
11	K,7,-W,L/2,H	
12	K,3,-W,0,H	
13	K,1,0,0,0	
14	K,5,0,L/2,0	
15	K,8,-W,L/2,0	
16	K,4,-W,0,0	
17	V,1,2,3,4,5,6,7,8	
18	ESIZE,0.00127	



19	VMESH, all	
20	DK,5,UX,0,,,UZ	! To prevent translation on the surface
21	DK,8,UZ,	! To prevent translation on the surface

Table B3: building a model for stress along X direction		
# of lines	Command	Comment
1	/FILENAME, SIGMAX	
2	/PREP7	! Weldments defined parameters
3	L=0.0254	! Weldment length
4	W=0.0762	! Weldment width
5	H=1.27E-2	! Weldment height
6	ET,1,SOLID186	
7	MP,EX,1, 2E11	! Young's Modulus
8	MP,PRXY,1,0.3	! Poisson's ratio
9	K,2,0,0,H	
10	K,6,0,L,H	
11	K,7,-W/2,L,H	
12	K,3,-W/2,0,H	
13	K,1,0,0,0	
14	K,5,0,L,0	
15	K,8,-W/2,L,0	
16	K,4,-W/2,0,0	
17	V,1,2,3,4,5,6,7,8	
18	ESIZE,0.00127	
19	VMESH,all	

20	DK,1,UY,0,,,UZ	
21	DK, 6, UZ,	

Table B4: Build a model for stress along Z direction		
# of lines	Command	Comment
1	/FILENAME, SIGMAZ	
2	/PREP7	! Weldments defined parameters
3	L=0.0254	! Weldment length
4	W=0.0762	! Weldment width
5	H=1.27E-2	! Weldment height
6	ET,1,SOLID186	
7	MP,EX,1, 2E11	! Young's Modulus
8	MP,PRXY,1,0.3	! Poisson's ratio
9	K,2,0,0,H/2	
10	K,6,0,L,H/2	
11	K,7,-W,L,H/2	
12	K,3,-W,0,H/2	
13	K,1,0,0,0	
14	K,5,0,L,0	
15	K,8,-W,L,0	
16	K,4,-W,0,0	
17	V,1,2,3,4,5,6,7,8	
18	ESIZE,0.00127	
19	VMESH, all	

20	DK,2,UX,0,,,UY	
21	DK,3,UY	

## APPENDIX C

### MAPLE CODING FOR DATA PROCESSING

This Appendix contains the coding in the software Maple to process the raw data obtained from Alicona. This includes, averaging data points, tilting the scanned surface, averaging two sets of data from two surfaces of the cut, applying Chebyshev polynomials, etc.

```
% Import data file into matrix G
```

```
GA := ImportMatrix(S4, source = auto, output = matrices); NmaxA := 132052.
```

```
GB := ImportMatrix(S4C, source = auto, output = matrices); NmaxB := 137482.
```

```
% Determining range of X, Y and Z coordinates
```

```
Xmin := 10^8; Xmax := -10^8; for m to NmaxA do if GA[m, 1] < Xmin then Xmin :=
```

```
GA[m, 1] end if end do; for m to NmaxA do if GA[m, 1] > Xmax then Xmax := GA[m, 1]
```

```
end if end do; XminA := Xmin; XmaxA := Xmax; Xmax-Xmin; Xmin := 10^8; Xmax := -
```

```
10^8; for m to NmaxB do if GB[m, 1] < Xmin then Xmin := GB[m, 1] end if end do; for
```

```
m to NmaxB do if GB[m, 1] > Xmax then Xmax := GB[m, 1] end if end do; XminB :=
```

```
Xmin; XmaxB := Xmax; Xmax-Xmin.
```

```
Ymin := 10^8; Ymax := -10^8; for m to NmaxA do if GA[m, 2] < Ymin then Ymin :=
```

```
GA[m, 2] end if end do; for m to NmaxA do if GA[m, 2] > Ymax then Ymax := GA[m, 2]
```

*end if end do; YminA := Ymin; YmaxA := Ymax; Ymax-Ymin; Ymin := 10^8; Ymax := -*  
*10^8; for m to NmaxB do if GB[m, 2] < Ymin then Ymin := GB[m, 2] end if end do; for*  
*m to NmaxB do if GB[m, 2] > Ymax then Ymax := GB[m, 2] end if end do; YminB :=*  
*Ymin; YmaxB := Ymax; Ymax-Ymin;*

*Zmin := 10^8; Zmax := -10^8; for m to NmaxA do if GA[m, 3] < Zmin then Zmin :=*  
*GA[m, 3] end if end do; for m to NmaxA do if GA[m, 3] > Zmax then Zmax := GA[m, 3]*  
*end if end do; Zmin; Zmax; Zmax-Zmin*

*Zmin := 10^8; Zmax := -10^8; for m to NmaxB do if GB[m, 3] < Zmin then Zmin :=*  
*GB[m, 3] end if end do; for m to NmaxB do if GB[m, 3] > Zmax then Zmax := GB[m, 3]*  
*end if end do; Zmin; Zmax; Zmax-Zmin*

*XminB := XmaxB-XmaxA+XminA*

*%Place origin of X and Y-axes into Xmin and Ymin*

*for m to NmaxA do GA[m, 1] := GA[m, 1]-XminA end do; for m to NmaxB do GB[m, 1]*  
*:= GB[m, 1]-XminB end do;*

*for m to NmaxA do GA[m, 2] := GA[m, 2]-YminA end do; for m to NmaxB do GB[m, 2]*  
*:= GB[m, 2]-YminB end do;*

*XmaxA := XmaxA-XminA; YmaxA := YmaxA-YminA; XmaxB := XmaxB-XminB; YmaxB*  
*:= YmaxB-YminB; XminA := 0; YminA := 0; XminB := 0; YminB := 0;*

*StepY := (Ymax-Ymin)\*(1/125); StepX := (Xmax-Xmin)\*(1/23)*

*R := (1/2)\*StepY*

*% Adjustment for tilting*

*% Determining Z values at 3 end points*

*x1 := 4\*StepX; y1 := 5\*StepY; Num := 0.1e-4; Zaver := 0; for k to NmaxA do if*

*abs(GA[k, 1]-x1) < R then if abs(GA[k, 2]-y1) < R then Zaver := Zaver+GA[k, 3]; Num*

*:= Num+1 end if end if end do; Num; z1 := Zaver/Num; x2 := 17\*StepX; y2 :=*

*5\*StepY; Num := 0.1e-4; Zaver := 0; for k to NmaxA do if abs(GA[k, 1]-x2) < R then if*

*abs(GA[k, 2]-y2) < R then Zaver := Zaver+GA[k, 3]; Num := Num+1 end if end if end*

*do; Num; z2 := Zaver/Num; x3 := 4\*StepX; y3 := 115\*StepY; Num := 0.1e-4; Zaver :=*

*0; for k to NmaxA do if abs(GA[k, 1]-x3) < R then if abs(GA[k, 2]-y3) < R then Zaver :=*

*Zaver+GA[k, 3]; Num := Num+1 end if end if end do; Num; z3 := Zaver/Num;*

*% Determining equation of plane passing through the end points*

*fsolve({z1 = b\*x1+c\*y1+a, z2 = b\*x2+c\*y2+a, z3 = b\*x3+c\*y3+a}, {a, b, c});*

*% Subtracting a+bx+cy from Z coordinate*

*for m to NmaxA do GA[m, 3] := -b\*GA[m, 1]-c\*GA[m, 2]-a+GA[m, 3] end do;*



```

x1 := 4*StepX; y1 := 5*StepY; Num := 0.1e-4; Zaver := 0; for k to NmaxB do if
abs(GB[k, 1]-x1) < R then if abs(GB[k, 2]-y1) < R then Zaver := Zaver+GB[k, 3]; Num
:= Num+1 end if end if end do; Num; z1 := Zaver/Num; x2 := 10*StepX; y2 :=
5*StepY; Num := 0.1e-4; Zaver := 0; for k to NmaxB do if abs(GB[k, 1]-x2) < R then if
abs(GB[k, 2]-y2) < R then Zaver := Zaver+GB[k, 3]; Num := Num+1 end if end if end
do; Num; z2 := Zaver/Num; x3 := 4*StepX; y3 := 115*StepY; Num := 0.1e-4; Zaver :=
0; for k to NmaxB do if abs(GB[k, 1]-x3) < R then if abs(GB[k, 2]-y3) < R then Zaver :=
Zaver+GB[k, 3]; Num := Num+1 end if end if end do; Num; z3 := Zaver/Num;

fsolve({z1 = bB*x1+cB*y1+aB, z2 = bB*x2+cB*y2+aB, z3 = bB*x3+cB*y3+aB}, {aB,
bB, cB});

for m to NmaxB do GB[m, 3] := -b*GB[m, 1]-c*GB[m, 2]-a+GB[m, 3]; do:

% Import mesh

M := ImportMatrix(mesh, source = auto, output = matrices);

NmaxM := 1941;

% Determining range of X, Y and Z coordinates

XminM := 10^8; XmaxM := -10^8; for m to NmaxM do if M[m, 4] < XminM then
XminM := M[m, 4] end if end do; for m to NmaxM do if M[m, 4] > XmaxM then XmaxM
:= M[m, 4] end if end do; XminM; XmaxM;

```

```

YminM := 10^8; YmaxM := -10^8; for m to NmaxM do if M[m, 2] < YminM then YminM
:= M[m, 2] end if end do; for m to NmaxM do if M[m, 2] > YmaxM then YmaxM :=
M[m, 2] end if end do; YminM; YmaxM;

```

```

% Matching data area with mesh and cutting off edge points

```

```

for m to NmaxA do GA[m, 1] := XminM+1.1*(GA[m, 1]-XminA)*(XmaxM-
XminM)/(XmaxA-XminA)-0.5e-1*(XmaxM-XminM) end do;

```

```

for m to NmaxA do GA[m, 2] := YminM+1.1*(GA[m, 2]-YminA)*(YmaxM-
YminM)/(YmaxA-YminA)-0.5e-1*(YmaxM-YminM) end do;

```

```

for m to NmaxB do GB[m, 1] := XminM+1.1*(GB[m, 1]-XminB)*(XmaxM-
XminM)/(XmaxB-XminB)-0.5e-1*(XmaxM-XminM) end do;

```

```

for m to NmaxB do GB[m, 2] := YminM+1.1*(GB[m, 2]-YminB)*(YmaxM-
YminM)/(YmaxB-YminB)-0.5e-1*(YmaxM-YminM) end do;

```

```

RX := (XmaxM-XminM)/(21*1.3); RY := (YmaxM-YminM)/(121*1.3);

```

```

for m to NmaxM do Num := 0.1e-4; Zaver := 0; for k to NmaxA do if abs(GA[k, 1]-
M[m, 4]) < RX then if abs(GA[k, 2]-M[m, 2]) < RY then Zaver := Zaver+GA[k, 3];
Num := Num+1 end if end if end do; Z := Zaver/Num; Num := 0.1e-4; Zaver := 0; for k
to NmaxB do if abs(GB[k, 1]-XmaxM+M[m, 4]) < RX then if abs(GB[k, 2]-M[m, 2]) <

```

```

RY then Zaver := Zaver+GB[k, 3]; Num := Num+1 end if end if end do; Z :=
1/2*(Z+Zaver/Num); print(m, Z, Num) end do;

B := array(1 .. 1, 1 .. 4);

for m to NmaxM do Num := 0.1e-4; Zaver := 0; for k to NmaxA do if abs(GA[k, 1]-
M[m, 4]) < RX then if abs(GA[k, 2]-M[m, 2]) < RY then Zaver := Zaver+GA[k, 3];
Num := Num+1 end if end if end do; Z := Zaver/Num; Num := 0.1e-4; Zaver := 0; for k
to NmaxB do if abs(GB[k, 1]-XmaxM+M[m, 4]) < RX then if abs(GB[k, 2]-M[m, 2]) <
RY then Zaver := Zaver+GB[k, 3]; Num := Num+1 end if end if end do; Z :=
1/2*(Z+Zaver/Num); B[1, 1] := M[m, 1]; B[1, 2] := M[m, 2]; B[1, 3] := Z; B[1, 4] :=
M[m, 4]; writedata[APPEND](Saverage, B); print(B[1, 1], B[1, 2], B[1, 3], B[1, 4],
Num) end do;

%%Smoothing by Chebyshev polynomials
for k to Nmax do G[k, 3] := 1 end do;

G := ImportMatrix(Saverage2, source = auto, output = matrices);

% Determining the range of X, Y coordinates
Xmin := 10^8; Xmax := -10^8; for m to Nmax do if G[m, 1] < Xmin then Xmin := G[m,
1] end if end do; for m to Nmax do if G[m, 1] > Xmax then Xmax := G[m, 1] end if end
do; Xmin; Xmax; Xmax-Xmin;

```

```

Ymin := 10^8; Ymax := -10^8; for m to Nmax do if G[m, 2] < Ymin then Ymin := G[m,
2] end if end do; for m to Nmax do if G[m, 2] > Ymax then Ymax := G[m, 2] end if end
do; Ymin; Ymax; Ymax-Ymin;

```

```

Zmin := 10^8; Zmax := -10^8; for m to Nmax do if G[m, 3] < Zmin then Zmin := G[m,
3] end if end do; for m to Nmax do if G[m, 3] > Zmax then Zmax := G[m, 3] end if end
do; Zmin; Zmax; Zmax-Zmin;

```

```

% Place origin of X and Y-axes into 0.5*(Xmin+Xmax) and 0.5*( Ymin+Ymax) and
rescale range of X and Y into [-1..1]

```

```

for m to Nmax do G[m, 2] := (2*G[m, 2]-Ymin-Ymax)/(Ymax-Ymin) end do;

```

```

M := 10;

```

```

C := array(0 .. M, 0 .. M);

```

```

% Calculation of expansion coefficients

```

```

N0 := 0; h := proc (X, Y) options operator, arrow; (1-X^2)^(1/2)*(1-Y^2)^(1/2) end
proc; for k to Nmax do N0 := N0+evalf(h(G[k, 1], G[k, 2])) end do; print(N0); N1 :=
1/evalf(16/(Pi^2*Nmax));

```

```

for n from 0 to M do for m from 0 to M do f := proc (X, Y) options operator, arrow; (1-
X^2)^(1/2)*(1-Y^2)^(1/2)*ChebyshevU(n, X)*ChebyshevU(m, Y) end proc; C[n, m] :=
0; for k to Nmax do C[n, m] := C[n, m]+evalf(G[k, 3]*f(G[k, 1], G[k, 2]))/N0 end do;
print(n, m, C[n, m]) end do end do;

```

```

% Calculation of smoothed Z values

for k to Nmax do Z := 0; for n from 0 to M do for m from 0 to M do f := proc (X, Y)
options operator, arrow; ChebyshevU(n, X)*ChebyshevU(m, Y) end proc; Z :=
Z+evalf(C[n, m]*f(G[k, 1], G[k, 2])) end do end do; G[k, 3] := Z end do;

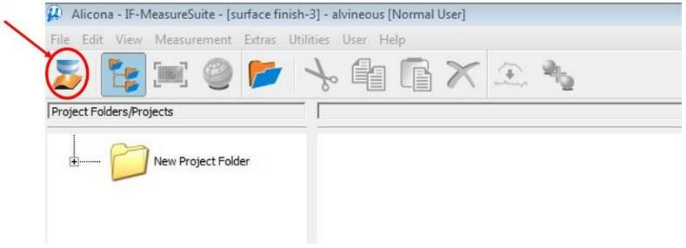
Zmin := 10^8; Zmax := -10^8; for m to Nmax do if G[m, 3] < Zmin then Zmin := G[m,
3] end if end do; for m to Nmax do if G[m, 3] > Zmax then Zmax := G[m, 3] end if end
do; Zmin; Zmax; Zmax-Zmin;

```

## APPENDIX D

### STEPS FOR OBTAINING DATA FROM ALICONA

This Appendix contains the step by step instructions of how to obtain data points from scanned surface in Alicona. This includes, determining the X, Y, Z ranges of the scan, importing data as text file, selecting the grid size, etc.

Steps:	Figures :
<p>Start the measurement by clicking on the circled icon as shown in Fig. D1.</p>	 <p>The screenshot shows the Alicona software window titled 'Alicona - IF-MeasureSuite - [surface finish-3] - alvineous [Normal User]'. The menu bar includes File, Edit, View, Measurement, Extras, Utilities, User, and Help. The toolbar contains various icons, with the 'New Project Folder' icon (a yellow folder) circled in red and pointed to by a red arrow. Below the toolbar, the 'Project Folders/Projects' pane shows a 'New Project Folder' icon.</p> <p>Fig. D1</p>

Change the setting of ImageField type to General ImageField as Fig. D2 shows (the red circle). The scanned surface needs three corners to locate the X, Y and Z range. Thus, three corners need to be taken for rough scan. Fig. D2 shows the scan of upper left corner. First step is to focus in the Z direction so the grain is clear.

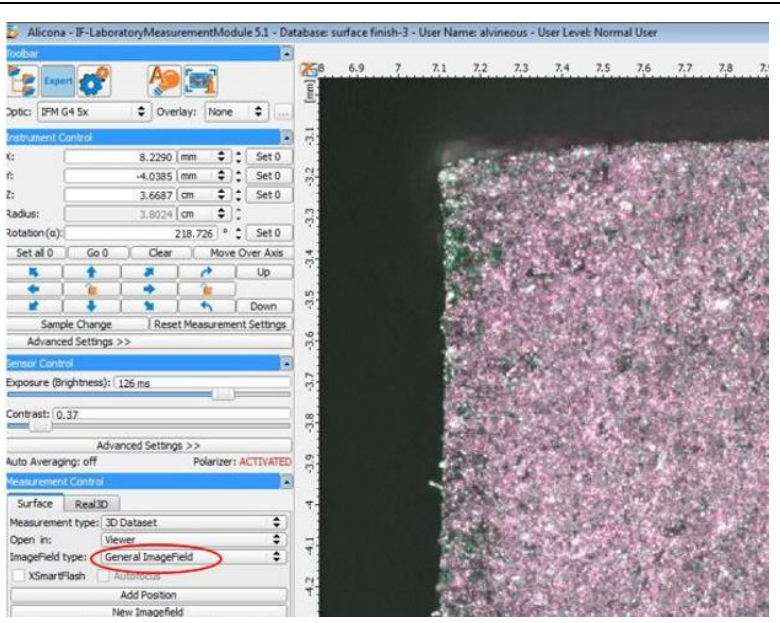


Fig. D2

Then moving up the lense will blur out the image as shown to the right. After moving up lense, the circled add position icon needs to be clicked to register this image (this includes X, Y coordinate and upper Z limit).

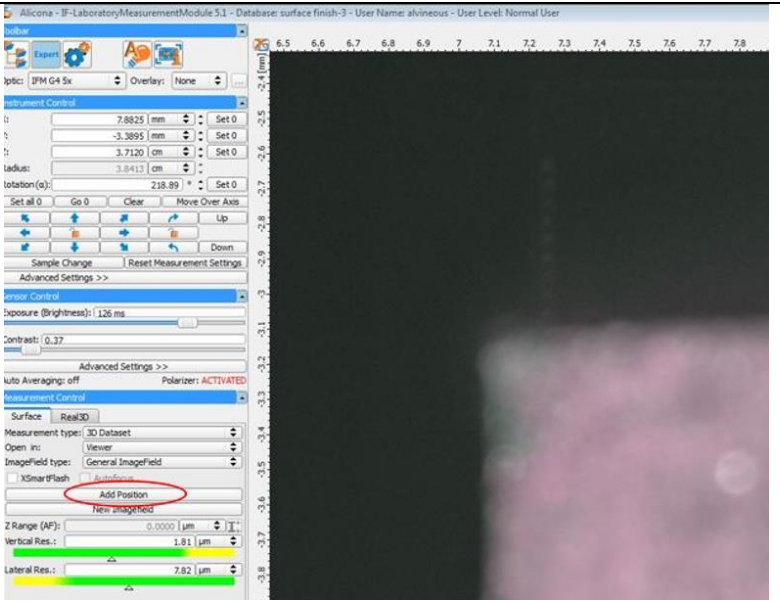


Fig. D3

Next step is to move to another corner (such as upper right corner) and lower the lense until it gets blurry.

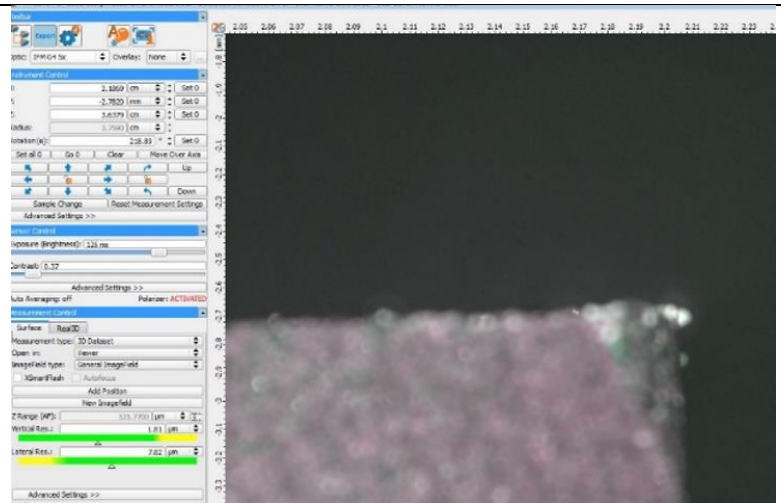


Fig. D4

Click the add position icon again and the X and Z range are thus determined. To determine the Y range, the lense is moved down to the third corner (such as lower right corner, shown to the right).

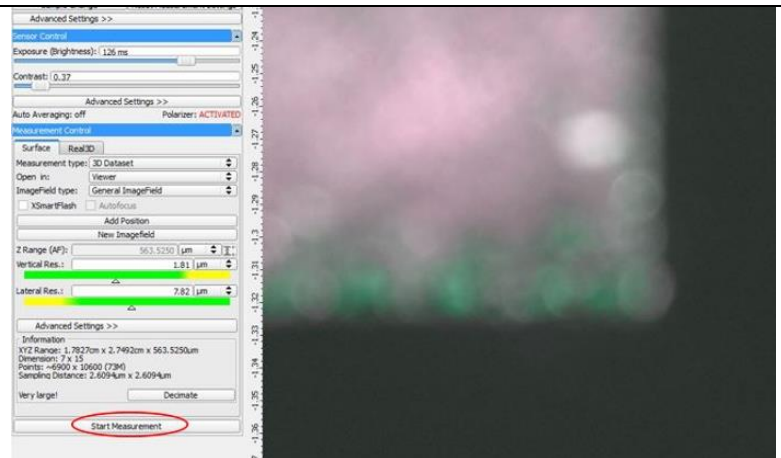


Fig. D5



So far, three corners have been scanned and X, Y and Z range have been determined. The next step is to click “start measurement” and the window shown to the right will pop up:

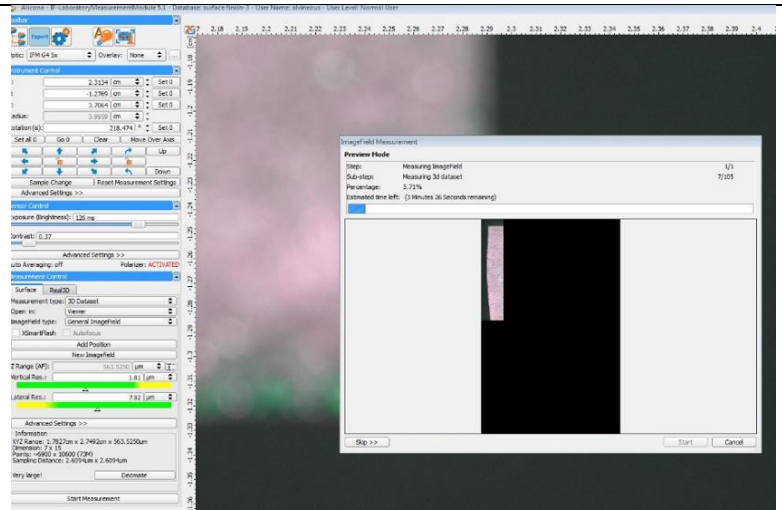


Fig. D6

The first scan is a quick/rough scan that locate the surface that needs to be scanned. This process usually takes within five minutes.

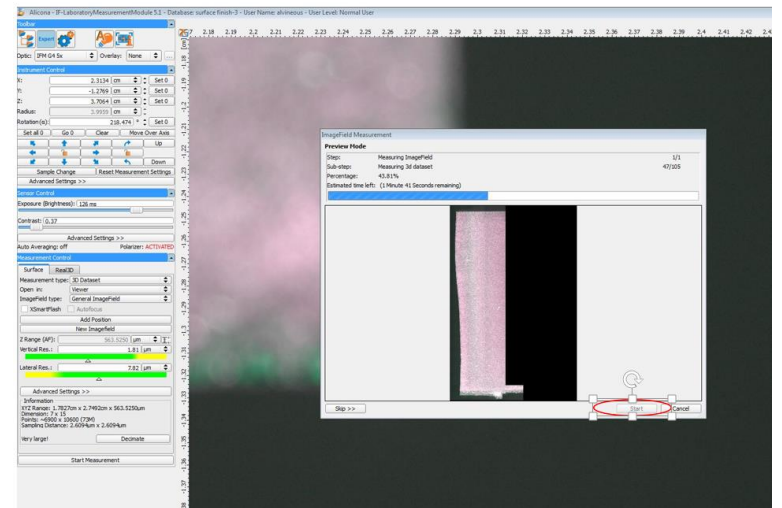


Fig. D7

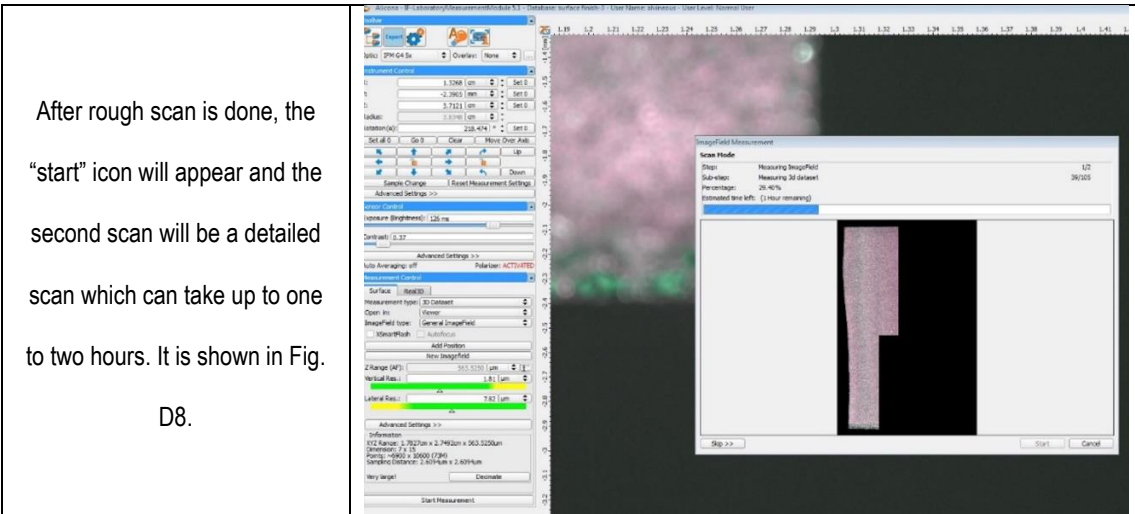


Fig. D8

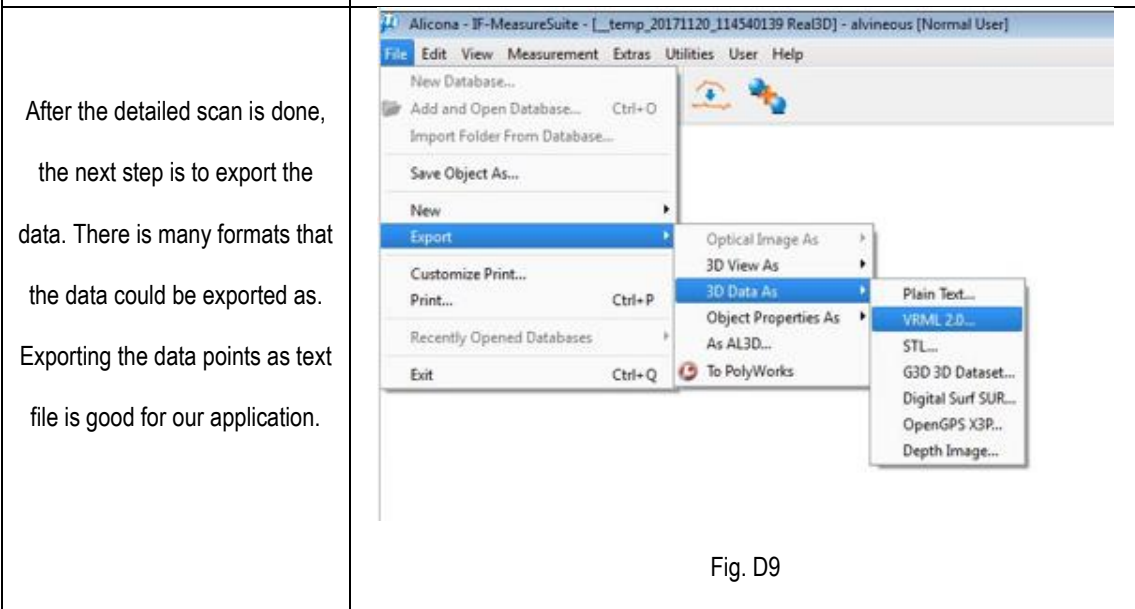


Fig. D9

To export the data points as plain text, go to File – Export – 3D Data As – Plain Text as previous picture shows. Then the picture to the right will pop up.

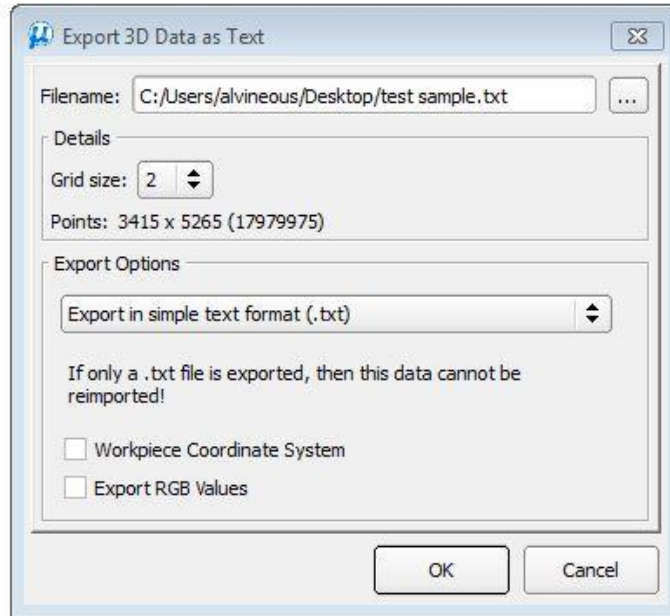


Fig. D10

Depending on the grid size chosen, the number of data points exported varies. When grid size is 2, 17979975 data points will be exported. This amount is normally not necessary. Therefore, a higher grid size (less data points) was selected as shown to the right

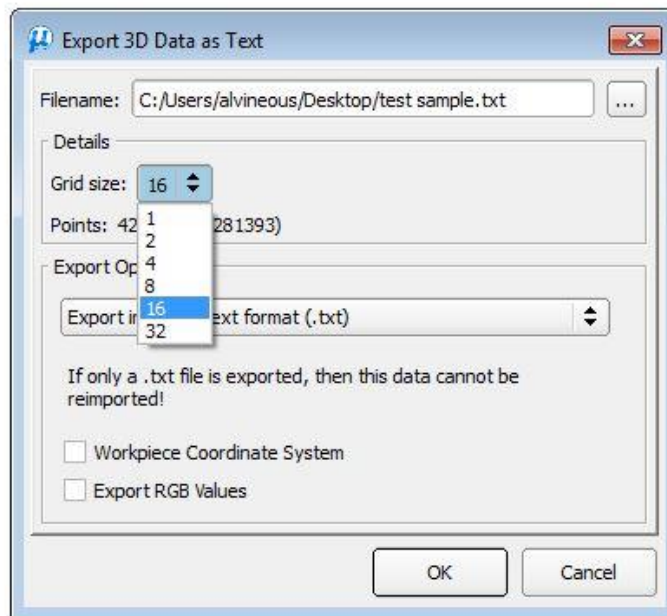


Fig. D11

When grid size is chosen as 32,  
70620 data points will be  
exported. This is more than  
enough for the mesh chosen.

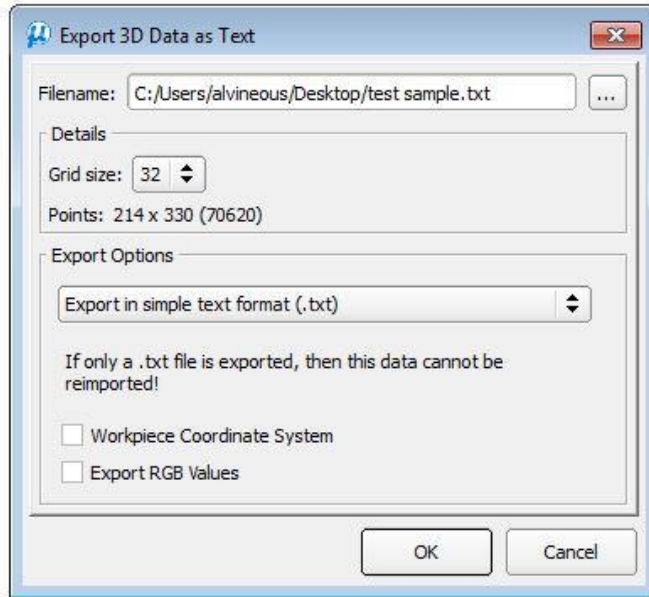


Fig. D12

## APPENDIX E

### EXPERIMENT FOR TESTING THE VALIDITY OF MAPLE CODING

This Appendix contains the procedures for testing the validity of the Maple program by setting up an experiment. One gage block was put under Alicona at an arbitrary angle on a clay (Fig. E1). We want to show that putting the data through the program can successfully tilt an inclined surface and confirm data manipulation from a flat to another flat surface.

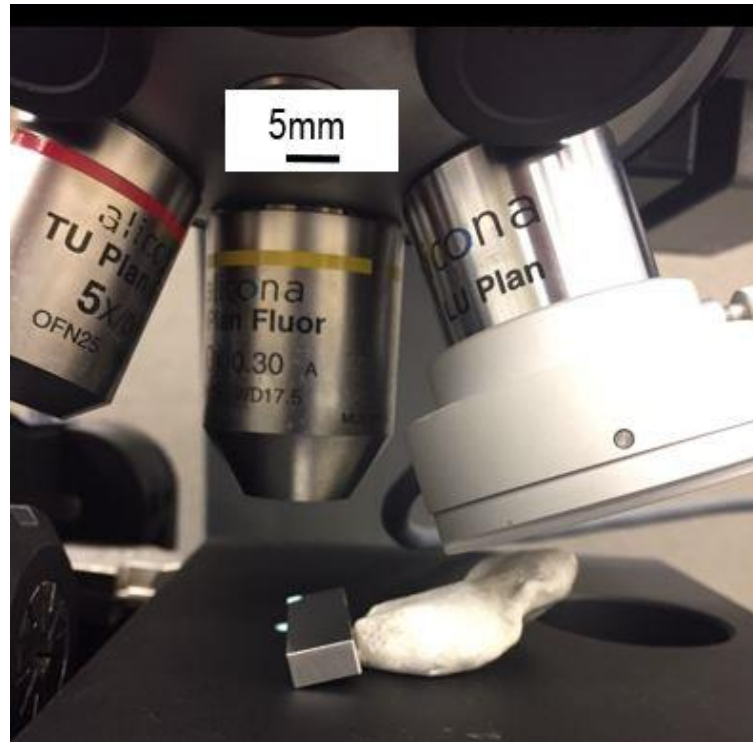


Figure. E1. Program calibration.

Since the tilted gage block is smooth on the top surface, the scanned contour would be a tilted surface. The gathered data points were first input into Matlab and 3D plot feature in Matlab was used to plot the surface contour. Then the data points were put through the program in Maple and the exported data points were plotted again in Matlab. The expected contour after tilting in Matlab should be a flat surface.

38586 data points were exported after scanning. Every data point contains X, Y and Z coordinate. They were plotted in Matlab as Fig. E2 shows.

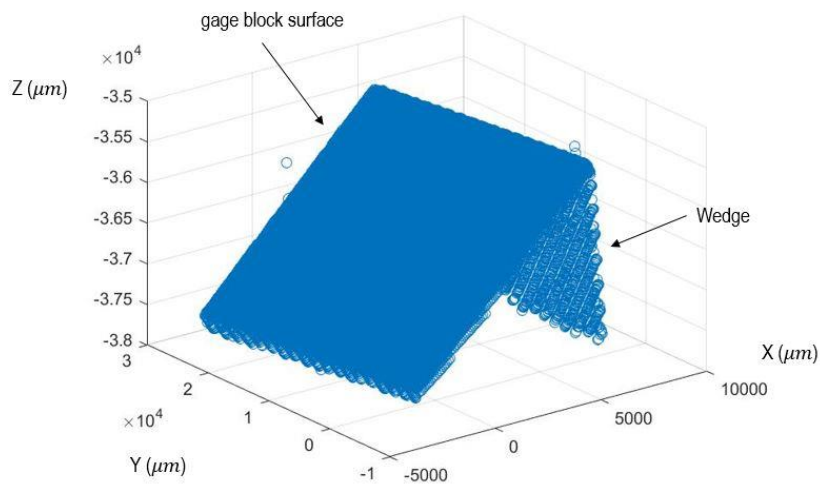


Figure. E2. Scanned contour before tilting

As Fig. E2 shows, the left incline is the gage block and the right side incline is part of the clay wedge that was used to support the gage block. But this has no effect since the left incline (gage block) was the focus of the experiment. The expected effect after putting the exported data into Maple program (Appendix C) was to make the left

incline “flat”. The “flat” here means that three points close to three corners were picked to generate a plane and all the scanned data points were then referenced off this plane, thus giving a flat surface parallel to  $XY$  plane. Since the top surface on gage block is indeed flat, the expected contour after tilting will be parallel to the  $XY$  plane. After the data points went through the Maple program, all 2956 data points were gathered and then plotted in Matlab:

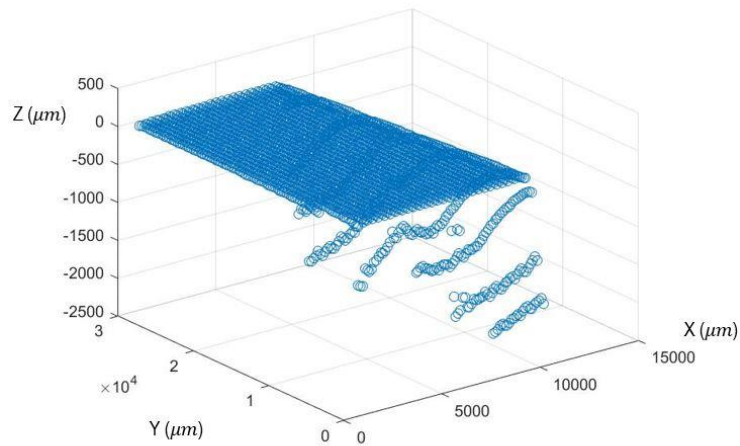


Figure. E3. Surface contour of the gage block after tilting.

It is very obvious that after the tilting (‘tilting’ here means that the scanned surface will be rotated to a certain degree so that the surface will be parallel to coordinate plane, in this case, it is the  $XY$  plane), the new contour is parallel to the  $XY$  plane and the new origin is set that allows for better observation. Thus, the Maple

program was shown to be able to (i) successfully tilt an inclined surface and (ii) confirm data manipulation from a flat to another flat surface.